
Unterschrift Betreuer



TECHNISCHE
UNIVERSITÄT
WIEN

DIPLOMARBEIT

Coherent Dynamics of a Spin Ensemble

Ausgeführt am
Atominstitut der Technischen Universität Wien
unter der Anleitung von

Univ. Prof. Dr. Hannes-Jörg Schmiedmayer
Univ. Ass. Dr. Johannes Majer
Projektass. Dipl.-Ing. Andreas Angerer

durch

Kirill Streltsov

Sturgasse 3-5
1020 Wien

Wien, 27. März 2017

Unterschrift Student

Abstract

In this thesis the theoretical and experimental treatment of the dynamics of a large ensemble of two-level systems that are equally coupled to a bosonic mode is presented. The connection to superradiance in open quantum systems is explored. The experimental system is based on a 3D cavity with a reduced mode volume and an ensemble of Nitrogen-Vacancy centers in diamond. With this system a coherent population inversion in a macroscopic ensemble is reached for the first time. The experiment is shown to agree well with the semiclassical theory.

Acknowledgements

I would like to thank my colleagues Andreas and Thomas for the many discussions that we had during my work on this thesis. I am also very thankful to Bill Munro, Kae Nemoto and Michael Trupke for the time they dedicated to discussions with me and the scientific guidance of my work. At a low point of this thesis I had the opportunity to visit the NanoQI summerschool where I had discussed the topic of this thesis with the organizer Prof. Geza Giedke. This discussion motivated me to strive for a deeper understanding of the topic and to produce more interesting results. I would also like to thank my supervisors Johannes Majer and Prof. Jörg Schmiedmayer for giving me the opportunity to work in the atomchip research group and attend the NanoQI summerschool. I learned many great things through the legendary coffee corner discussions of the atomchip group that reach far beyond physics related topics.

This thesis would not have been possible without the studies that preceded it. I am very thankful to my friends and colleagues from and with whom I studied throughout the last years. Their passion for physics was a constant source of inspiration for me.

I would also like to express my gratitude to my friends Christoph, Stefanie, Florian, Sarah and Anna who have always been there for me through the many ups and downs of the last years. Without them this thesis would not have been possible. Last but not least I would like to thank my mother for the support that she has given me throughout my life.

Contents

| | |
|---|-----------|
| 1. Introduction | 1 |
| 1.1. Superradiant Laser | 2 |
| 1.2. Relevance for Other Quantum Technologies | 4 |
| 1.3. Conventions and Notation | 5 |
| 2. Theory | 7 |
| 2.1. Jaynes-Cummings Model | 7 |
| 2.1.1. Rotating Wave Approximation | 8 |
| 2.1.2. Solution | 9 |
| 2.1.3. Dynamics | 10 |
| 2.2. Tavis-Cummings Model | 11 |
| 2.2.1. Approximations | 14 |
| 2.3. Master Equation | 16 |
| 2.4. Maxwell-Bloch Equations | 18 |
| 2.4.1. Numerical Analysis for a Single Emitter | 22 |
| 2.5. Superradiance - Coherent Spontaneous Emission | 25 |
| 2.5.1. Dicke's Thought Experiment | 25 |
| 2.5.2. Coherence | 27 |
| 2.5.3. Superradiance in Vacuum | 29 |
| 2.5.4. Classical Aspects of Superradiance | 32 |
| 2.5.5. Maxwell-Bloch Equations for Multiple Emitters | 34 |
| 3. Experimental System | 37 |
| 3.1. The Nitrogen Vacancy Defect Center in Diamond | 37 |
| 3.1.1. Level Structure | 38 |
| 3.2. 3D Cavity | 39 |
| 4. Experimental Results | 45 |
| 4.1. Measurement Scheme | 45 |
| 4.2. Inversion of the NV^- ensemble | 47 |
| 5. Conclusion | 53 |
| A. Relation of the Exponential Decay to the Cavity Linewidth | 55 |
| Bibliography | 57 |

1. Introduction

Quantum mechanics is to this day one of the main topics of fundamental research in physics. Over its history it has not only changed our understanding of the world but also was of technological relevance. The laser is an example for a high impact application of quantum mechanics. The transistor can also be considered to be a quantum technology as well as imaging methods based on nuclear magnetic resonance and advanced sensors based on the properties of superconductors (SQUID).

In this work we will explore the phenomenon of superradiance which was first predicted in 1954 [1] and is now enjoying renewed interest because of its relevance for a new type of laser [2]. Furthermore, the superradiant phase transition [3, 4] is now experimentally accessible [5, 6]. The first theoretical publications about superradiance were focused on introducing the idea of superradiance in vacuum and proposing experiments that would show that effect. However, there were also publications that looked at superradiance in a closed system [7]. In modern publications, that often focus on experimental realizations, these cases are sometimes mixed which leads to misleading interpretations or presentations of results.

In this thesis we will introduce the theoretical concepts that are necessary for the treatment of superradiance and provide an intuitive explanation of the effect. Furthermore, we establish the connection to the dynamics of a classical dipole and explain the difference between superradiance in vacuum and in a cavity. In the experimental part of this thesis we study the dynamics of a highly excited ensemble of Nitrogen-Vacancy centers which corresponds to the case of superradiance in a closed system. Shortly before this thesis was completed a preprint was published [8] where the authors conduct very similar experiments as in this thesis. However, the presentation suffers from the aforementioned inaccuracies on which the treatment in this thesis can hopefully provide some clarity.

The original idea for this thesis was to build a variation of a superradiant maser as proposed in [9]. However, due to the cryogenic setting of our experiment and the required strong optical pumping this proposal was not pursued further. In the following section a short description of the superradiant laser is provided because it constitutes the main motivation to pursue research related to superradiance.

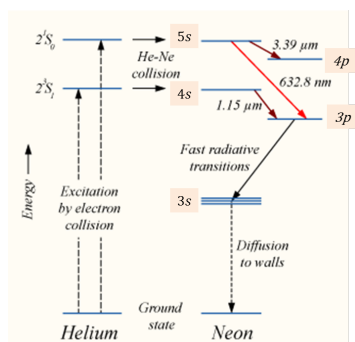


Figure 1.1.: Level scheme for the Helium-Neon laser.

1.1. Superradiant Laser

The defining feature of a laser is the coherence of emitted radiation, i.e. the emission spectrum has a narrow linewidth. Among other applications this property is important for the measurement of time in atomic clocks [10–12], the detection of gravity waves [13] and ground state cooling of nanomechanical oscillators [14].

A conventional laser consists of an incoherently pumped gain medium that is located within a high finesse cavity. In the first laser, that could produce continuous output, the gain medium was a Helium-Neon gas mixture that was confined in a discharge tube. The Helium atoms were excited by collisions with the electrons that were produced by the discharge tube. Then Helium atoms transferred energy to the Neon atoms through collisions, which then radiatively decayed. The energy level scheme for this setup is depicted in fig. 1.1. In such a setup the photons are emitted in all directions with random phases because the medium is far larger than the wavelength of the radiation and the Neon atoms are uniformly spread out over the whole volume.

The second important component of a laser is the cavity. It captures the photons that are in a specific spatial mode, thereby increasing the population of this mode. The presence of photons in the cavity mode leads to stimulated emission, i.e. a preferred decay of the gain medium into this mode. Therefore, the cavity is similar to a filter. The spectral linewidth of the cavity determines the linewidth of the laser. Current state of the art lasers are limited by thermal fluctuations of the cavity mirrors to linewidths of 0.125-0.3 Hz [15, 16]. One way to mitigate this effect is to use cryogenic single-crystal cavities [17]. Another is to make the gain medium emit coherent radiation directly. This coherent spontaneous emission is also called superradiance [2].

Superradiant or bad-cavity lasers are based on atomic ensembles that are confined in optical lattices which are placed inside a cavity. However, in this case the cavity mirrors must have a relatively high transmission rate and the average photon number in the cavity mode should be $\ll 1$. As one can guess from this requirement, stimulated emission plays a subordinate role in this concept. Instead, the effect of superradiance that leads to the collective enhancement of the

dipole moment of a collection of atoms, is exploited.

As Dicke showed in 1954 [1], excited atoms that are separated by a distance that is smaller than the wavelength of the emitted radiation, decay faster than the same number of excited atoms that are far apart. This effect emerges because the atoms don't decay independently but coherently. As will be shown in section 2.5.3, this means that the rate of photon emission scales with N^2 , where N is the number of atoms. This allows one to directly extract photons from ultranarrow clock transitions at sufficiently high intensities. For example, the spontaneously emitted radiation on the clock transition of 10^6 fully inverted and independent ^{87}Sr atoms is of the order of 10^{-16} Watt. If these atoms are coerced into emitting coherently, the power increases to 10^{-12} Watt [2], which is sufficient to use this radiation as a frequency reference.

The condition, that the atoms must be separated by a distance that is not larger than the wavelength, requires one to make a very small cloud of atoms that has a very high density to obtain sufficiently high output intensities. However, this requirement can be relaxed by capturing relatively small numbers of atoms on the sites of an optical lattice which is located inside a cavity. It was shown that if the lattice sites coincide with the antinodes of the cavity mode and if the cavity decay rate is not too large, correlations can emerge between atoms on different lattice sites. The latter requirement is also called the collective strong coupling regime.

The theoretical proposal was implemented in a Raman system [18] as a proof of principle. In this case however, the frequency stability is limited by the stability of the Raman lasers. Recently, superradiance of an ensemble of ^{87}Sr atoms, trapped in an optical lattice and enclosed by a cavity, was shown [19]. However, no steady state superradiant laser on an ultranarrow clock transition has been experimentally implemented yet.

There are many variants of optical atomic clocks that offer promising improvements over current generation clocks that operate in the microwave regime. Besides frequency stability one might also be interested in clocks that are less complex and thus cheaper and easier to deploy.

Optical lasers had an exceptional impact on science and industry since their invention. However, the very first "laser" was operated in the microwave regime - and was called maser for that matter. This type of lasers did not have as big of an impact because of their immense complexity. They are either implemented in atomic or free-electron systems that require vacuum chambers and pumping. Solid state implementations on the other hand require cryogenic cooling. It has been a long quest to build a room-temperature maser based on a solid state system. Oxborrow et. al. demonstrated an implementation based on an organic mixed molecular crystal in 2012 [20]. Unfortunately, organic materials can only produce low output powers. The superradiant laser proposal led to the idea of a maser based on Nitrogen-Vacancy centers in a diamond [9] that is not only simple to implement but also allows relatively high output powers.

1.2. Relevance for Other Quantum Technologies

The explanation of the effects that were discussed so far requires an understanding of quantum mechanics, but the experimental realization does not require the control of single quantum systems. In the history of quantum mechanics such a high level of control was long considered to be impossible. Schrödinger famously wrote [21]:

„We never experiment with just one electron or atom or (small) molecule. In thought-experiments we sometimes assume that we do; this invariably entails ridiculous consequences... we are not experimenting with single particles, any more than we can raise Ichthyosauria in the zoo.“

With the birth of Cavity Quantum Electrodynamics (CQED)[22] such level of control became a reality and theorists began to think about how some of the "ridiculous consequences" could be technologically exploited. This is the time when first ideas about quantum computation emerged and culminated in a paper by David Deutsch [23], that described a universal quantum computer. The quest for an experimental realization of these ideas led to the development of many experimental implementations of qubits (the basic building blocks of a quantum computer), of which the superconducting qubit seems to be the most promising one. The ability to control and engineer single quantum systems is believed to lead to a second generation of quantum technologies that will have a great impact in the areas of communication, computation and metrology.

While we do not deal with single quantum systems in this thesis, the theoretical treatment and our experimental system are still relevant for the second generation of quantum technologies. It was proposed that an ensemble of Nitrogen-Vacancy centers [24, 25] or atoms [26] can serve as a quantum memory. Such a device was experimentally implemented [27] in a similar system as was used for the experiments in this thesis. In fact, a study of the spectral properties of the Nitrogen-Vacancy centers and superradiance [25] was a necessary prerequisite for the implementation of the quantum memory. However, the experimental protocols might still be improved by considering the recently demonstrated cavity protection effect [28] or by employing spectral hole burning to mitigate the effects of inhomogeneous broadening [29]. But it should be noted that systems based on superconducting qubits [30] or single ^{13}C nuclear spins in the vicinity of a Nitrogen-Vacancy center in diamond [31] so far show superior properties for the use as quantum memories.

1.3. Conventions and Notation

In this thesis we use the usual definitions of the Pauli and ladder operators

$$\sigma^z = \begin{pmatrix} 1 & 0 \\ 0 & -1 \end{pmatrix}, \quad \sigma^x = \begin{pmatrix} 0 & 1 \\ 1 & 0 \end{pmatrix}, \quad \sigma^y = \begin{pmatrix} 0 & -i \\ i & 0 \end{pmatrix}, \quad \sigma^\pm = \frac{1}{2}(\sigma_x \pm i\sigma_y). \quad (1.1)$$

With

$$\begin{aligned} \sigma^z |\uparrow\rangle &= |\uparrow\rangle, & \sigma^z |\downarrow\rangle &= -|\downarrow\rangle, \\ \sigma^+ |\downarrow\rangle &= |\uparrow\rangle, & \sigma^- |\uparrow\rangle &= |\downarrow\rangle, \\ \sigma^+ |\uparrow\rangle &\equiv 0, & \sigma^- |\downarrow\rangle &\equiv 0. \end{aligned}$$

The commutation relations are given by

$$[\sigma^a, \sigma^b] = 2i\epsilon_{abc}\sigma^c, \quad [\sigma^z, \sigma^\pm] = \pm 2\sigma^\pm. \quad (1.2)$$

The collective operators

$$J_\pm = \sum_{i=1}^N \sigma_i^\pm, \quad J_z = \sum_{i=1}^N \sigma_i^z. \quad (1.3)$$

are denoted with the usual symbol for angular momentum operators but omit the factor $\hbar/2$ that is common in the the angular momentum formalism. Therefore, the commutation relations for the collective spin operators are equivalent to the ones of the Pauli matrices and thus slightly different than in the angular momentum formalism. Furthermore, the definition of the ladder operator has an additional factor of $1/2$

$$J_\pm = \frac{1}{2}(J_x \pm J_y). \quad (1.4)$$

The eigenfunctions and eigenvalues of these operators can be defined as [32, Chapter 6.2]

$$J^2 |j, m\rangle = j(j+1) |j, m\rangle, \quad J_z |j, m\rangle = 2m |j, m\rangle, \quad a^\dagger a |n\rangle = n |n\rangle. \quad (1.5)$$

With

$$\begin{aligned} J^2 |j, m\rangle &= \left(\frac{1}{2}J_x\right)^2 + \left(\frac{1}{2}J_y\right)^2 + \left(\frac{1}{2}J_z\right)^2 \\ &= \frac{1}{2}(J_+J_- + J_-J_+) + \frac{1}{4}J_z^2. \end{aligned} \quad (1.6)$$

The operator signs were omitted where their omittance doesn't lead to confusion. Vectors are denoted as **bold face** symbols. The absolute values of vector quantities are denoted by the same symbol as the vector but in regular face.

2. Theory

In this chapter we will introduce the theoretical tools that are needed to describe the phenomenon of superradiance. First, we introduce basic models of light matter interaction in closed systems in section 2.1 and section 2.2. Then, we provide an introduction to the master equation which is used to model open quantum systems. Based on it we derive the Maxwell-Bloch equations that model light matter interaction in open quantum systems. In the last part of this chapter we introduce the phenomenon of superradiance and discuss its phenomenology in vacuum and in closed systems.

2.1. Jaynes-Cummings Model

One of the simplest models of light-matter interaction is the Jaynes-Cummings model [33]. To derive the Jaynes-Cummings model we start with a Hamiltonian that describes a two-level system - referred to as "atom" in the following - that is dipole-coupled to an oscillating field

$$\begin{aligned} H &= H_{field} + H_{atom} + H_{int} \\ &= \hbar\omega_c a^\dagger a + \frac{\hbar\omega_a}{2} \sigma_z - \frac{\hbar\Omega}{2} (\sigma^+ + \sigma^-)(a^\dagger + a). \end{aligned} \quad (2.1)$$

To be able to write the kinetic energy term of the atom as proportional to σ_z we assume that there is a static external field that defines the quantization axis. We can now choose the field amplitude of the bosonic mode to be facing in some perpendicular direction to the static field and choose our coordinate system such that this direction corresponds to the x axis. Note that this needs to be an oscillating field because a static field in the x direction would simply tilt the quantization axis. If the oscillating field has a z component, i.e. a component in the direction of the static field, then the energy of the dipole transition becomes time dependent. However, as we will see shortly, this fluctuation of the transition energy can be neglected in a certain parameter regime.

In the interaction picture the equation of motion for an operator, that is time-independent in the Schrödinger picture, is given by

$$\frac{dO_I}{dt} = \frac{i}{\hbar} [H_0, O_I], \quad (2.2)$$

with H_0 denoting the non-interacting part of the Hamiltonian. Thus, in the interaction picture $\sigma_I^+(t) = \sigma^+ e^{i\omega_a t}$, $\sigma_I^-(t) = \sigma^- e^{-i\omega_a t}$, $a_I^\dagger(t) = a^\dagger e^{i\omega_c t}$, $a_I(t) =$

$ae^{-i\omega_c t}$. The Hamiltonian in the interaction picture reads

$$H_I = -\frac{\hbar\Omega}{2}(\sigma^+ a^\dagger e^{i(\omega_a + \omega_c)t} + \sigma^- a^\dagger e^{-i(\omega_a - \omega_c)t} + \sigma^+ a e^{i(\omega_a - \omega_c)t} + \sigma^- a e^{-i(\omega_a + \omega_c)t}). \quad (2.3)$$

Note that the interaction picture is used to separate the part of the Hamiltonian (H_0) for which an exact solution is known. This part might contain interaction terms. In this case one can not say that the time evolution of a product of two operators is the product of the time evolutions of each individual operator as we did above.

The Hamiltonian in eq. (2.3) can equivalently be written as

$$\begin{aligned} H_I &= -\frac{\hbar(\omega_c - \omega_a)}{2}\sigma_z - \frac{\hbar\Omega}{2}(\sigma^+ a^\dagger e^{i2\omega_c t} + \sigma^- a^\dagger + \sigma^+ a + \sigma^- a e^{-i2\omega_c t}) \\ &= \hbar(\omega_c - \omega_a)a^\dagger a - \frac{\hbar\Omega}{2}(\sigma^+ a^\dagger e^{i2\omega_a t} + \sigma^- a^\dagger + \sigma^+ a + \sigma^- a e^{-i2\omega_a t}). \end{aligned} \quad (2.4)$$

To obtain this form one sets the frequency of the atom equal to the frequency of the field in H_0 and to compensate for that adds a term that is proportional to the difference of the frequencies to the interaction Hamiltonian (with the correct sign). The derivation of these expressions can be done with eq. (2.2). Or, even more generally, with the help of the Hadamard-Lemma

$$e^X Y e^{-X} = \sum_{m=0}^{\infty} \frac{1}{m!} [X, Y]_m$$

with $[X, Y]_m = [X, [X, Y]_{m-1}]$ and $[X, Y]_0 = Y$.

2.1.1. Rotating Wave Approximation

There are terms in the Hamiltonian that oscillate with the summed frequency $\omega_a + \omega_c$ and those that oscillate with the difference frequency $\omega_a - \omega_c$. In the case that the field is in resonance with the atom, i.e. $\omega_a \approx \omega_c$, and that $\Omega \ll \omega_a$ as well as $\Omega\sqrt{n+1} \ll \omega_a$, with n denoting the number of excitations in the bosonic mode, we can apply the Rotating Wave Approximation (RWA) and neglect the terms that oscillate with the sum of the angular frequencies.

We will not provide a full proof of the validity of the RWA but instead give a short intuitive example. Starting from the equation of motion in the interaction picture

$$\frac{d}{dt} |\psi(t)\rangle_I = -\frac{i}{\hbar} H_I(t) |\psi(t)\rangle_I,$$

we obtain the time evolution operator in the interaction picture

$$U_I(t) = \exp \left[-\frac{i}{\hbar} \int_0^t H_{int}(\tau) d\tau \right]. \quad (2.5)$$

In the case of the Jaynes-Cummings model the relevant timescale for the integral in eq. (2.5) is given by the inverse of the coupling constant Ω scaled with the number of photons to $\Omega\sqrt{n+1}$. Thus, if the interaction Hamiltonian contains terms that are oscillating on a far smaller timescale than that, they average to zero under the integral. This is the reason why - in a regime where the RWA is valid - it is acceptable if the driving mode has a component in the direction of the quantization axis. Such a setup will have a term like $H_{int} = \sigma_z(a^\dagger + a)$. Since σ_z is constant in the interaction picture such an interaction term oscillates with the frequency of the bosonic mode in the interaction picture and can thus be neglected if the RWA is valid.

A recent state of the art circuit QED experiment (cavity QED with electrical circuits) has reached a regime where $\Omega \approx \omega_a$ [34]. Alternatively, this parameter regime can also be reached in effective systems [6]. In both cases the RWA can not be applied anymore.

2.1.2. Solution

Applying the RWA to eq. (2.3) and transforming back into the Schrödinger picture we obtain the Jaynes-Cummings Hamiltonian

$$H_{JC} = \hbar\omega_c a^\dagger a + \frac{\hbar\omega_a}{2}\sigma_z - \frac{\hbar\Omega}{2}(\sigma^+ a + \sigma^- a^\dagger). \quad (2.6)$$

We can now look at this Hamiltonian in the product basis of Fock and spin states $|n, \uparrow\rangle$. One can see that the interaction term is degenerate with respect to $|n, \uparrow\rangle$ and $|n+1, \downarrow\rangle$, i.e. the Hamiltonian has a block diagonal form. The subspace with a total of n excitations that are shared between the atom and the bosonic mode looks like

$$H^{(n)} = \hbar \begin{bmatrix} n\omega_c + \frac{\omega_a}{2} & \frac{\Omega}{2}\sqrt{n+1} \\ \frac{\Omega}{2}\sqrt{n+1} & (n+1)\omega_c - \frac{\omega_a}{2} \end{bmatrix}.$$

There are two non-degenerate eigenvalues of $H^{(n)}$

$$E_{\pm}(n) = \hbar\omega_c \left(n + \frac{1}{2} \right) \pm \frac{1}{2}\hbar\Omega_n(\Delta) \quad (2.7)$$

with $\Delta = \omega_c - \omega_a$ and $\Omega_n(\Delta) = \sqrt{\Delta^2 + \Omega^2(n+1)}$. The eigenvectors are

$$|n, +\rangle = \sin\left(\frac{\alpha_n}{2}\right) |n+1, \downarrow\rangle + \cos\left(\frac{\alpha_n}{2}\right) |n, \uparrow\rangle, \quad (2.8)$$

$$|n, -\rangle = \cos\left(\frac{\alpha_n}{2}\right) |n+1, \downarrow\rangle - \sin\left(\frac{\alpha_n}{2}\right) |n, \uparrow\rangle, \quad (2.9)$$

with $\alpha_n = \tan^{-1} \left(\frac{\Omega\sqrt{n+1}}{\Delta} \right)$. These states are often referred to as dressed atomic states. When the two-level system and the bosonic mode are in resonance, i.e. $\omega_c = \omega_a$, the eigenstates are given by

$$|n, \pm\rangle = \frac{1}{\sqrt{2}} (|n+1, \downarrow\rangle \pm |n, \uparrow\rangle). \quad (2.10)$$

2.1.3. Dynamics

The time evolution of an arbitrary initial state $|\psi(0)\rangle$ can now be computed by projecting $|\psi(0)\rangle$ onto the states in eqs. (2.8) and (2.9).

$$\begin{aligned} |\psi(t)\rangle = \sum_{n=0}^{\infty} & \left(\exp\left(-\frac{i}{\hbar} E_+^{(n)} t\right) \langle\psi(0)|n, +\rangle |n, +\rangle \right. \\ & \left. + \exp\left(-\frac{i}{\hbar} E_-^{(n)} t\right) \langle\psi(0)|n, -\rangle |n, -\rangle \right). \end{aligned} \quad (2.11)$$

For an initial number state in the bosonic mode $|\psi(0)\rangle = |n+1, \downarrow\rangle$ and $\omega_c = \omega_a$ we get

$$|\psi(t)\rangle = \cos\left(\frac{\Omega_n t}{2}\right) |n+1, \downarrow\rangle + \sin\left(\frac{\Omega_n t}{2}\right) |n, \uparrow\rangle. \quad (2.12)$$

For a finite detuning $\Delta = \omega_c - \omega_a$ this expression changes to

$$\begin{aligned} |\psi(t)\rangle &= \exp\left(-i\frac{\Omega_n t}{2}\right) \sin\left(\frac{\alpha_n}{2}\right) |n, +\rangle + \exp\left(i\frac{\Omega_n t}{2}\right) \cos\left(\frac{\alpha_n}{2}\right) |n, -\rangle \\ &= \left(\exp\left(-i\frac{\Omega_n t}{2}\right) \sin\left(\frac{\alpha_n}{2}\right)^2 + \exp\left(i\frac{\Omega_n t}{2}\right) \cos\left(\frac{\alpha_n}{2}\right)^2 \right) |n+1, \downarrow\rangle - \\ &\quad - 2i \sin\left(\frac{\Omega_n t}{2}\right) \cos\left(\frac{\alpha_n}{2}\right) \sin\left(\frac{\alpha_n}{2}\right) |n, \uparrow\rangle \\ &= \left(\cos\left(\frac{\Omega_n t}{2}\right) + i \cos\left(\frac{\Omega_n t}{2}\right) \sin\left(\frac{\alpha_n}{2} t\right) \right) |n+1, \downarrow\rangle - \\ &\quad - i \sin\left(\frac{\Omega_n t}{2}\right) \sin\left(\frac{\alpha_n}{2} t\right) |n, \uparrow\rangle. \end{aligned} \quad (2.13)$$

It is immediately obvious that in the resonant case an occupation probability of 1 can be reached in the excited state of the atom while this is not possible in the off-resonant case. However, in the off-resonant case this probability can get arbitrarily close to 1 if the number of excitations in the bosonic mode is large.

For brevity we will omit the explicit expressions of the time dependent wave function for the case of a coherent initial state in the bosonic mode. They are given by superpositions of eq. (2.13). The dynamics for this case are depicted

in fig. 2.1. No matter whether the bosonic mode is on resonance or not a deterministic " π -pulse" is not possible if the bosonic mode is initially in a coherent state. But the fidelity can be made arbitrary high by increasing the field intensity (however, one should always keep in mind that the rotating wave approximation will break down at some point). Whenever the bosonic mode is not in a specific number state the solution is a superposition of multiple oscillations.

2.2. Tavis-Cummings Model

An extension of the Jaynes-Cummings model is the Tavis-Cummings model [35] where one considers N two-level systems that are coupled to one bosonic mode. Relative phases and interactions between the emitters are neglected in this model, therefore it is better suited to describe a single higher-spin quantum system or many two-level systems that are very close to each other, i.e. whose spatial wave functions overlap. The Hamiltonian is a straightforward generalization of eq. (2.6)

$$\begin{aligned} H_{JC} &= \hbar\omega_c a^\dagger a + \frac{\hbar\omega_a}{2} \sum_i^N \sigma_i^z - \hbar g \sum_i^N (\sigma_i^+ a + \sigma_i^- a^\dagger) \\ &= \hbar\omega_c a^\dagger a + \frac{\hbar\omega_a}{2} J_z - \hbar g (J_+ a + J_- a^\dagger) \end{aligned} \quad (2.14)$$

Where we have used the collective operators defined in section 1.3. Their eigenstates and eigenvalues are defined as

$$J^2 |j, m\rangle = j(j+1) |j, m\rangle, \quad J_z |j, m\rangle = 2m |j, m\rangle, \quad a^\dagger a |n\rangle = n |n\rangle. \quad (2.15)$$

The free and interaction parts of the Hamiltonian commute. Therefore, it is possible to find a basis that will diagonalize both parts simultaneously. The eigenstates of the full Tavis-Cummings Hamiltonian can be labeled by j and $c = n+m$ where n denotes the number of photons and m one half of the eigenvalue of the J_z operator (see section 1.3). Note that $-j \leq c < \infty$. The eigenstates of the Tavis-Cummings Hamiltonian can be written as a superposition of the eigenstates of the free part

$$|j, c, i\rangle = \sum_{n=c-j}^{c+j} A_n^{(j,c,i)} |n\rangle |j, c-n\rangle. \quad (2.16)$$

Here i is merely a label to distinguish states that have the same j and c . The full solution is derived in [35]. The eigenstates of the Tavis-Cummings system are dressed states of a spin $N/2$ system just like the Jaynes-Cummings eigenstates are dressed states of a spin $1/2$ system. However, the number of states within each rung of the energy ladder now increases with the number of excitations in the system till it reaches the maximal value $2j+1$ as is obvious from the sum

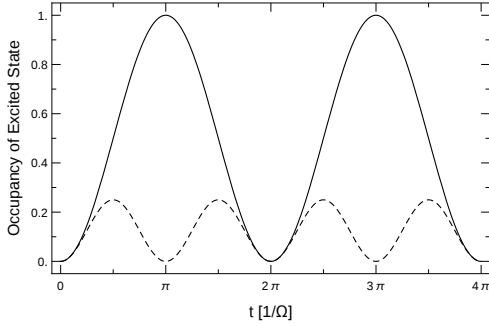
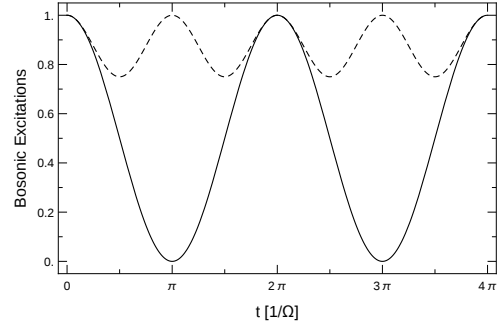
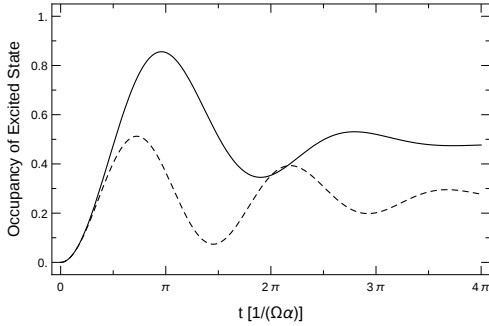
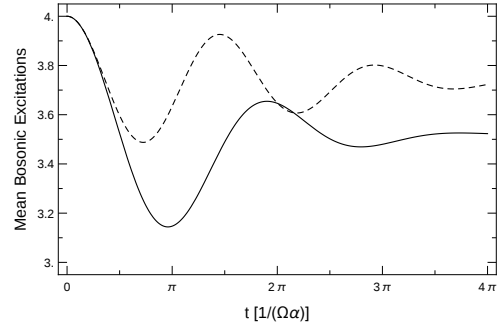
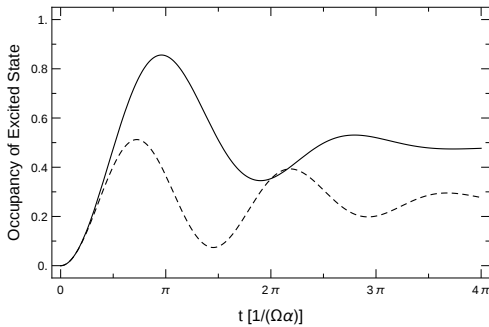
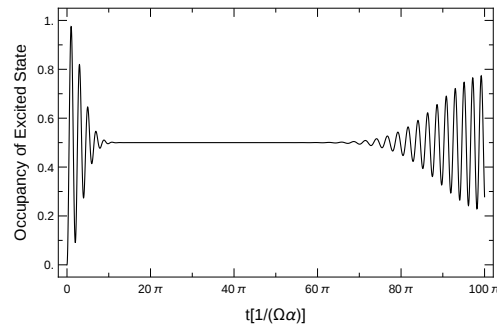
(a) Occupancy of the excited state of the two level system for $|\psi(0)\rangle = |1, \downarrow\rangle$.(b) Mean number of excitations in the bosonic mode for $|\psi(0)\rangle = |1, \downarrow\rangle$.(c) Occupancy of the excited state of the two level system for a coherent initial state in the bosonic mode $|\psi(0)\rangle = |\alpha = 2, \downarrow\rangle$.(d) Mean number of excitations in the bosonic mode for a coherent initial state in the bosonic mode $|\psi(0)\rangle = |\alpha = 2, \downarrow\rangle$.(e) Occupancy of the excited state of the two level system for a coherent state with $\alpha = 5$.(f) Occupancy of the excited state of the two level system for a coherent state with $\alpha = 5$.

Figure 2.1.: Dynamics of the Jaynes-Cummings model for different initial conditions. Solid line: bosonic mode and two level system in resonance. Dashed line: bosonic mode and two level system detuned with $\Delta = \sqrt{3}\Omega$.

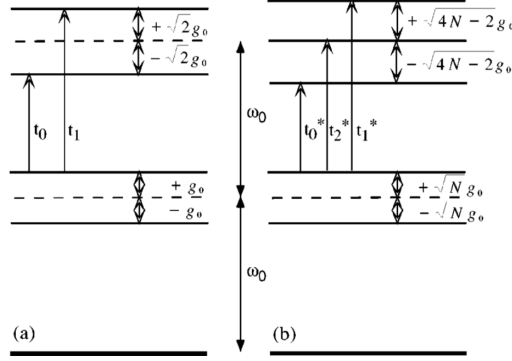


Figure 2.2.: Energy level structure of the first two excited states of the Jaynes-Cummings (left) and Tavis-Cummings model with N two-level systems (right). For $N \gg 1$ the transitions t_1^* and t_2^* are at $\omega_0 + g\sqrt{N}$ and $\omega_0 - g\sqrt{N}$ respectively. The transition t_0^* is highly suppressed which makes the ladder harmonic for $N \gg 1$. The figure is reproduced from [36].

in eq. (2.16). The energy level structure for the Jaynes-Cummings and Tavis-Cummings models are compared in fig. 2.2.

To illustrate some of the properties of the Tavis-Cummings model we present the eigenstates for a few special cases. For a single excitation of the system $c = -j + 1$, thus the sum in eq. (2.16) has only two terms. This corresponds to the first rung of the dressed ladder that consists of two states which we label with $-$ and $+$

$$|j, 1, \pm\rangle = \frac{1}{\sqrt{2}}(|1\rangle |j, m = -j\rangle \pm |0\rangle |j, m = j\rangle). \quad (2.17)$$

The eigenenergies for these states are

$$E_{\pm} = \hbar\omega_c \pm \sqrt{N}\hbar g \quad (2.18)$$

Note that we have set the ground state energy to 0 instead of the usual $\hbar\omega_c/2$. For completeness we write the angular momentum eigenstates in the individual emitter basis (sometimes referred to as the computational basis)

$$|j, m = -j\rangle = |\downarrow, \downarrow, \dots, \downarrow\rangle, \quad |j, m = -j + 1\rangle = \frac{1}{\sqrt{N}} \sum_i^N |\downarrow, \dots, \uparrow_i, \dots, \downarrow\rangle. \quad (2.19)$$

In quantum information theory the latter state is referred to as the "W-state". For a system that consists of two emitters each rung of the ladder will have

maximally three states. These states are given by [37]

$$\begin{aligned}
|j = 1, c, 0\rangle &= \sqrt{\frac{c+1}{2c+1}} |J = 1, m = 1\rangle |c-1\rangle - \sqrt{\frac{c}{2c+1}} |J = 1, m = -1\rangle |c+1\rangle, \\
|j = 1, c, \pm 1\rangle &= \sqrt{\frac{c}{2(2c+1)}} |J = 1, m = 1\rangle |c-1\rangle \\
&\quad + \sqrt{\frac{c+1}{2(2c+1)}} |J = 1, m = -1\rangle |c+1\rangle \pm \sqrt{\frac{1}{2}} |J = 1, m = 0\rangle |c\rangle,
\end{aligned} \tag{2.20}$$

it is implied that the number of excitations is at least two and thus $c \geq 1$. The eigenenergies for these states are

$$E_{c,0} = (c+1)\hbar\omega_c, \quad E_{c,\pm 1} = (c+1)\hbar\omega_c \pm 2\hbar g \sqrt{c + \frac{1}{2}}. \tag{2.21}$$

Here, g denotes the single two-level system coupling. A discussion of the energy spectrum of the Tavis-Cummings model can be found in [36].

2.2.1. Approximations

Experimental realizations of the Tavis-Cummings model often feature high numbers of emitters as well as high occupation numbers of the bosonic mode. One would expect that in both of these cases the system approaches a classical limit in some sense. In this section we will explore various approximations for the Tavis-Cummings model.

The first approximation is based on the Holstein-Primakoff transformation [38]

$$J_+ = b^\dagger \sqrt{2j - (b^\dagger b)}, \quad J_- = \sqrt{2j - (b^\dagger b)} b, \quad J_z = b^\dagger b. \tag{2.22}$$

This transformation is exact. It transforms an ensemble of non-interacting two-level systems into an interacting bosonic system. The correspondence between the bosonic and the spin states is given by

$$|j, m = -j + n\rangle = |n\rangle. \tag{2.23}$$

For a small number of excitations relative to the total number of emitters, i.e. $\langle b^\dagger b \rangle \ll j$, the bosons are interacting only weakly and the Holstein-Primakoff *approximation* can be made

$$J_+ = b^\dagger \sqrt{2j} \sqrt{1 - \frac{b^\dagger b}{2j}} \approx b^\dagger, \quad J_- = \sqrt{2j} \sqrt{1 - \frac{b^\dagger b}{2j}} b \approx b, \quad J_z = b^\dagger b. \tag{2.24}$$

This transforms the Tavis-Cummings model into a model of two interacting bosonic modes. An analytical solution for such a system exists not only in the case of Hamiltonian dynamics, but also when decay channels are introduced [39].

Another limit to consider is the high excitation limit where $c \gg j$. The implications of it become obvious when looking at the states in eq. (2.20). The contributions from the $|j = 1, m = 1\rangle$ and $|j = -1, m = -1\rangle$ states become symmetric

$$\begin{aligned} |j = 1, c, 0\rangle &\approx \sqrt{\frac{1}{2}} |J = 1, m = 1\rangle |c\rangle - \sqrt{\frac{1}{2}} |J = 1, m = -1\rangle |c\rangle, \\ |j = 1, c, \pm 1\rangle &\approx \sqrt{\frac{1}{4}} |J = 1, m = 1\rangle |c\rangle + \sqrt{\frac{1}{4}} |J = 1, m = -1\rangle |c\rangle \\ &\pm \sqrt{\frac{1}{2}} |J = 1, m = 0\rangle |c\rangle, \end{aligned} \quad (2.25)$$

The dynamics of the spin part of the wave function for the cases $c = j$ and $c \gg j$ are plotted in fig. 2.3. For the case $c \gg j$ we have also added the dynamics of 3 two-level systems that are directly driven by a classical field with amplitude η . Such a setup is described by

$$H = \frac{\hbar\omega}{2} J_z + \hbar g \eta (J_+ e^{-i\omega t} + J_- e^{i\omega t}). \quad (2.26)$$

The solution to this Hamiltonian is given by the spin coherent state

$$|\psi(t)\rangle = \prod_{i=1}^3 (\cos(gt) |\uparrow\rangle_i + \sin(gt) |\downarrow\rangle_i), \quad (2.27)$$

The dynamics of the emitter ensemble increasingly resembles the dynamics of independently driven two level systems as it is given by the spin coherent state. Note that this statement is independent of the coupling strength g . A proper comparison of the time evolution due to the Tavis-Cummings Hamiltonian and the spin coherent state would require us to trace over the bosonic states which would give us a mixed state which is classified by N^2 complex numbers. However as eq. (2.25) suggests, with increasing c the total wave function looks similar to a product of the emitter state and the state of the bosonic mode. Tracing over the bosonic states in this case produces a pure emitter state with N real coefficients. Therefore, the comparison in fig. 2.3 where we only plot the time evolution of the occupation probabilities of the basis states, is valid.

We have discussed the limits of very low and very high bosonic excitation. An other interesting limit is the case where the number of two-level systems is very large. The level splittings of the ladder of eigenstates arise due to the interaction term $(J_+ a + J_- a^\dagger)$ and since J_\pm are nonlinear operators we expect to get an additional anharmonicity in addition to the \sqrt{n} anharmonicity of the bosonic operators in the Jaynes-Cummings model. Keeling [40] explores the scaling of this anharmonicity and finds that it decreases with the number of two-level systems albeit very slowly. He concludes that the effects due to the anharmonicity are still relevant even for 10^6 emitters.

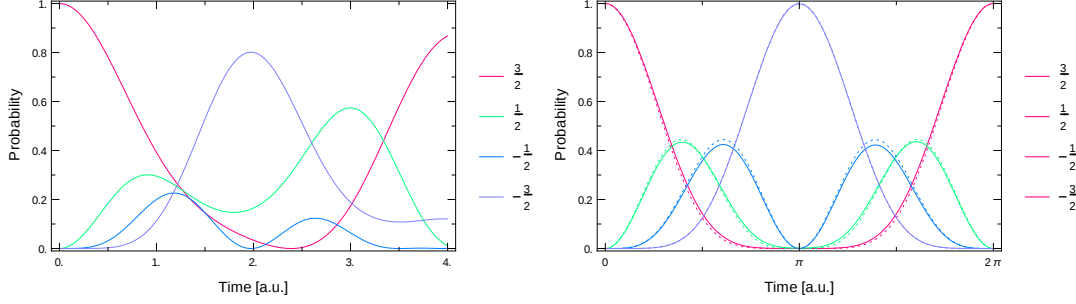


Figure 2.3.: Time dependent occupation probabilities of the different collective emitter states $|j, m\rangle$ for the cases $c = j$ (left) and $c = 2j + 20$ (right). The dotted lines in the right panel show the solution to eq. (2.26).

One further approximation that is relevant for the study of the Tavis-Cummings model is the semiclassical approximation. It is applicable when the single emitter coupling g is small. In this case all operator correlation functions are replaced by the single operator expectation values, i.e. all quantum correlations are neglected. As pointed out in [40] the semiclassical approximation also amounts to assuming that the spacing between the energy eigenstates within each subspace of constant c of the dressed energy ladder is equal, i.e. that there is no anharmonicity. This approximation will be further discussed in section 2.4.

2.3. Master Equation

So far we have discussed closed quantum systems whose time evolution is governed by unitary Hamiltonian dynamics. However, any real system will not be perfectly isolated from the environment. In this case it is called an open quantum system. Similar to classical systems with dissipative channels its dynamics will be damped. The correct way to introduce damping in a quantum system is through the means of the master equation, since a naive introduction of a damping term in the equations of motion of quantum operators would make their commutation relations decay in time. We can only provide a short introduction to the topic here and the interested reader is referred to the excellent treatment in [41] which we follow closely.

In the following we use the subscript S to label operators that live in the Hilbert space of the system and R to label the operators of the reservoir, i.e. the environment. We start with the observation that the expectation values of system operators only depend on the density matrix of the system

$$\langle O_S \rangle = Tr_{S \otimes R}(O_S \chi(t)) = Tr_S(O_S Tr_R(\chi(t))) = Tr_S(O_S \rho(t)). \quad (2.28)$$

Where we have identified the partial trace of the full density matrix $\chi(t)$ to

correspond to the system density matrix

$$\rho(t) = Tr_R(\chi(t)). \quad (2.29)$$

To determine the time evolution of $\rho(t)$ we write the full Hamiltonian

$$H = H_S + H_R + H_{SR}. \quad (2.30)$$

H_{SR} contains the interaction terms between the system and the reservoir. The time evolution of the full density matrix in the interaction picture

$$\tilde{\chi}(t) = e^{(i/\hbar)(H_S+H_R)t} \chi(t) e^{-(i/\hbar)(H_S+H_R)t}, \quad (2.31)$$

is given by

$$\dot{\tilde{\chi}}(t) = -\frac{i}{\hbar} [\tilde{H}_{SR}(t), \tilde{\chi}(t)]. \quad (2.32)$$

Formal integration of this equation yields

$$\tilde{\chi}(t) = \tilde{\chi}(0) - \frac{i}{\hbar} \int_0^t dt' [\tilde{H}_{SR}(t'), \tilde{\chi}(t')]. \quad (2.33)$$

Plugging this back into eq. (2.32) gives

$$\dot{\tilde{\chi}}(t) = -\frac{i}{\hbar} [\tilde{H}_{SR}(t), \chi(0)] - \frac{1}{\hbar^2} \int_0^t dt' [\tilde{H}_{SR}(t), [\tilde{H}_{SR}(t'), \tilde{\chi}(t')]]. \quad (2.34)$$

If the reservoir couples weakly to the system and if it is sufficiently large we can assume that the density operator of the reservoir remains constant over time. We denote it as R_0 and assume that the full density matrix at $t = 0$ is a product of the density matrices of the system and the reservoir. Then the full time-dependent density matrix has the following form

$$\tilde{\chi}(t) = \tilde{\rho}(t) \tilde{R}_0 + \mathcal{O}(\tilde{H}_{SR}(t)). \quad (2.35)$$

We can further assume that $Tr_R(H_{SR}(t)R_0) = 0$ because if this is not the case this term can always be absorbed in the definition of the system density matrix. We can now plug eq. (2.35) into eq. (2.34), take the partial trace over the reservoir and neglect terms higher than second order in \tilde{H}_{SR} , obtaining

$$\dot{\tilde{\rho}}(t) = -\frac{1}{\hbar^2} \int_0^t dt' [\tilde{H}_{SR}(t), [\tilde{H}_{SR}(t'), \tilde{\rho}(t') \tilde{R}_0]]. \quad (2.36)$$

This is referred to as the *Born approximation*. Another approximation that is commonly applied is the *Markov approximation*. One assumes that the interaction with the reservoir only depends on the current system state, i.e. $\tilde{\rho}(t')$ is replaced with $\tilde{\rho}(t)$ yielding the *master equation in the Born-Markov approximation* [32, Eq. 1.31]

$$\dot{\tilde{\rho}}(t) = -\frac{1}{\hbar^2} \int_0^t dt' [\tilde{H}_{SR}(t), [\tilde{H}_{SR}(t'), \tilde{\rho}(t) \tilde{R}_0]]. \quad (2.37)$$

The Markov approximation is only valid if the changes introduced to the reservoir due to the interaction with the system, decay faster than the timescale on which $\tilde{\rho}(t)$ varies. To continue further one has to specify more details about the reservoir and H_{SR} . We assume linear coupling in the system operators

$$H_{SR} = \hbar \sum_i s_i \Gamma_i, \quad (2.38)$$

where s_i denotes system operators and Γ_i the reservoir operators including coupling constants. If the open quantum system under study is a harmonic oscillator this term looks like

$$H_{SR} = \hbar \sum_i (a r_i^\dagger + a^\dagger r_i) = \hbar (a \Gamma^\dagger + a^\dagger \Gamma). \quad (2.39)$$

In the course of the further derivation we have to evaluate correlation functions of the environment operators which will require us to make assumptions about the density of states of the environment and the occupation of these states due to finite temperature. Furthermore it turns out that the coupling to the environment changes the unitary time evolution. In the case of a two-level system or atom coupled to the environment this corresponds to the Lamb shift and a temperature dependent frequency shift that can be interpreted as an AC-Stark shift due to the thermal photons. For brevity the derivation is omitted here and the reader is again encouraged to follow the treatment in [32]. We only state the final result for a finite temperature environment that consists of harmonic oscillators. In the Schrödinger picture, neglecting the changes to the unitary time evolution due to the coupling to the environment, the time evolution of the system density matrix is governed by

$$\dot{\rho} = -\frac{i}{\hbar} [H_S, \rho] + \sum_i \frac{\gamma_i}{2} (\bar{n}+1) (2s_i \rho s_i^\dagger - s_i^\dagger s_i \rho - \rho s_i^\dagger s_i) + \sum_i \frac{\gamma_i}{2} \bar{n} (2s_i^\dagger \rho s_i - s_i s_i^\dagger \rho - \rho s_i s_i^\dagger). \quad (2.40)$$

Indeed, there exists a proof that the most general equation that preserves the trace of ρ must be of *Lindblattform*

$$\dot{\rho} = -\frac{i}{\hbar} [H_S, \rho] + \sum_i \frac{\Gamma_i}{2} (2s_i \rho s_i^\dagger - s_i^\dagger s_i \rho - \rho s_i^\dagger s_i). \quad (2.41)$$

2.4. Maxwell-Bloch Equations

In experiments one measures expectation values of operators because the quantum mechanical wave functions are not directly accessible. Therefore, it is interesting to derive the equations of motion for some of these quantities. For the Jaynes-Cummings model, these equations together with the semiclassical approximation, i.e. $\langle \hat{A}\hat{B} \rangle = \langle \hat{A} \rangle \langle \hat{B} \rangle$, are called the Maxwell-Bloch equations (MBE).

The semiclassical approximation in this context is sometimes also referred to as the mean field approximation.

The Maxwell-Bloch equations are usually derived in the rotating frame. Since it is easily confused with the interaction picture we shortly explain the difference in the following. In the interaction picture one splits the Hamiltonian $H = H_0 + H_{int}$ into two parts and transforms it according to

$$H_I = e^{iH_0t/\hbar} H e^{-iH_0t/\hbar}. \quad (2.42)$$

The time evolution of the operators is governed by H_0 according to

$$\dot{O}_I = \frac{i}{\hbar} [H_0, O_I], \quad (2.43)$$

as already stated in eq. (2.2). While the evolution of the density matrix is governed by H_I

$$\dot{\rho}_I = -\frac{i}{\hbar} [H_I, \rho_I]. \quad (2.44)$$

This ensures that the expectation values are the same as in the Schrödinger picture $\langle O \rangle = Tr(O\rho) \equiv Tr(O_I\rho_I)$. The rotating frame on the other hand is introduced to make the time dependent terms in the Hamiltonian time independent. For the example of a Jaynes-Cummings model where the bosonic mode is coherently driven with an oscillating classical field with angular frequency ω_d

$$H_{JC} = \hbar\omega_c a^\dagger a + \frac{\hbar\omega_a}{2} \sigma_z - \frac{\hbar\Omega}{2} (\sigma^+ a + \sigma^- a^\dagger) + \eta (a^\dagger e^{-i\omega_d t} + a e^{i\omega_d t}), \quad (2.45)$$

the transformation into the rotating frame is given by (note the ω_d dependence)

$$H_R = e^{i\omega_d a^\dagger a + \frac{\omega_d}{2} \sigma_z} H e^{-i\omega_d a^\dagger a + \frac{\omega_d}{2} \sigma_z}, \quad (2.46)$$

yielding the Hamiltonian in the rotating frame

$$H_R = \hbar\Delta_c a^\dagger a + \frac{\hbar\Delta_a}{2} \sigma_z - \frac{\hbar\Omega}{2} (\sigma^+ a + \sigma^- a^\dagger) + \eta (a^\dagger + a). \quad (2.47)$$

However, now the operators and the density matrix evolve according to the same Hamiltonian H_R , i.e. the formalism is the same as in the Schrödinger picture and *not* like in the interaction picture. The expectation values of operators are different and one has to be careful when comparing theoretical results with experimental data (see footnote in section 3.2).

To derive the Maxwell-Bloch equations we start with an open quantum system whose unitary dynamics are described by the Tavis-Cummings model and that has various loss channels. We start with the master equation and model the loss channels with Lindblat terms. We will furthermore assume that the temperature of the environment is low enough so that the thermal occupation of energy levels around $\hbar\omega$ is zero ($\bar{n} = 0$ in eq. (2.40)). The cavity damping is described by

$$\mathcal{L}_{cavity}(\rho) = \kappa(2a\rho a^\dagger - a^\dagger a\rho - \rho a^\dagger a). \quad (2.48)$$

We also introduce a non-radiative spontaneous decay channel for the emitters. In a solid this models the process where an excited emitter decays and produces a lattice excitation. We assume that the damping acts on each emitter individually, which is why we use the single emitter operators σ^- instead of J_- in the Lindblatt term, obtaining

$$\mathcal{L}_{decay}(\rho) = \gamma_{\parallel} \sum_i^N (2\sigma_i^- \rho \sigma_i^+ - \sigma_i^+ \sigma_i^- \rho - \rho \sigma_i^+ \sigma_i^-), \quad (2.49)$$

where N denotes the number of emitters. There can also be purely phase destroying processes like elastic collisions in atomic vapor or elastic phonon scattering. We can model these processes with the following Lindblatt term

$$\mathcal{L}_{dephasing}(\rho) = \gamma_{\perp} \sum_i^N (2\sigma_i^z \rho \sigma_i^z - 2\rho), \quad (2.50)$$

where we have used the property $\sigma^z \sigma^z = \mathbb{1}$. This term is purely phenomenological and its form is determined by the requirement that it should not affect the expectation value of $\dot{\sigma}^z = Tr(\sigma^z \dot{\rho})$, i.e. it should not lead to decay.

Beside dephasing and decay an excitation channel of the system should be included. One way to do that is to flip the sign on the terms that cause decay. This approach is used to model incoherent pumping. This way of modeling pumping is useful if one considers only a part of the quantum system in the Hamiltonian evolution but uses other parts to excite it. This can be a three level system of which only the levels one and two are relevant for the unitary evolution but a transition from the first to the third level, which consequently decays to the second, is used to excite the system.

A system can also be driven coherently which means that a transition is excited directly. Such a driving term leaves the system in a pure state which is why it is usually written as a part of the Hamiltonian. An example for a driven bosonic mode would be

$$H_{drive} = i\hbar\eta \cos(\omega_d t)(a^\dagger - a). \quad (2.51)$$

And with the rotating wave approximation applied

$$H_{drive} = i\hbar\eta(a^\dagger e^{-i\omega_d t} - a e^{i\omega_d t}). \quad (2.52)$$

The drive strength η can be related to the power of the drive by $\eta = \sqrt{\kappa_{drive} P}$, where κ_{drive} is the coupling of the drive to the bosonic mode and P denotes the power (or amplitude squared) of the drive. Further details are provided in section 3.2.

The full Hamiltonian is given by

$$H = \hbar\omega_c a^\dagger a + \frac{\hbar\omega_a}{2} J_z + ig(a^\dagger J_- - a J_+) + i\hbar\eta(a^\dagger e^{-i\omega_d t} - a e^{i\omega_d t}). \quad (2.53)$$

Transforming into the rotating frame and assuming $\omega_d = \omega_a = \omega_c$ we obtain

$$H = ig(a^\dagger J_- - a J_+) + i\hbar\eta(a^\dagger - a). \quad (2.54)$$

The corresponding master equation is

$$\begin{aligned} \dot{\rho} = & g[a^\dagger J_- - a J_+, \rho] - i\eta[a^\dagger + a, \rho] + \kappa(2a\rho a^\dagger - a^\dagger a\rho - \rho a^\dagger a) \\ & + \gamma_{\parallel} \sum_i^N (2\sigma_i^- \rho \sigma_i^+ - \sigma_i^+ \sigma_i^- \rho - \rho \sigma_i^+ \sigma_i^-) + \gamma_{\perp} \sum_i^N (2\sigma_i^z \rho \sigma_i^z - 2\rho). \end{aligned} \quad (2.55)$$

Now we can write the equations of motion for the expectation values of all relevant operators by using the property $\langle \hat{O} \rangle = Tr(\hat{O}\hat{\rho})$ and $\langle \dot{\hat{O}} \rangle = Tr(\dot{\hat{O}}\hat{\rho})$. For the last relation to hold true we need to be in the Schrödinger picture because we need to commute the time derivative and the operator \hat{O} . We obtain [41, Chapter 15 and 16]

$$\langle \dot{a} \rangle = -\kappa \langle a \rangle + g \langle J_- \rangle + \eta \quad (2.56)$$

$$\langle \dot{a}^\dagger \rangle = -\kappa \langle a^\dagger \rangle + g \langle J_+ \rangle + \eta \quad (2.57)$$

$$\langle \dot{J}_- \rangle = -(\gamma_{\parallel} + \gamma_{\perp}) \langle J_- \rangle + g \langle J_z a \rangle \quad (2.58)$$

$$\langle \dot{J}_+ \rangle = -(\gamma_{\parallel} + \gamma_{\perp}) \langle J_+ \rangle + g \langle J_z a \rangle \quad (2.59)$$

$$\langle \dot{J}_z \rangle = -2\gamma_{\parallel}(\langle J_z \rangle + 1) - 2g(\langle J_+ a \rangle + \langle J_- a^\dagger \rangle) \quad (2.60)$$

Note that the factor $2g$ in the last equation depends on the convention that one uses for the collective operators. This is not a closed set of equations since there are new expectation values like $\langle J_z a \rangle$ whose equations of motion we need to add to the above set. These additional equations will contain higher order correlations and the process will continue till the equations for all possible correlation functions are derived. This set will quickly become prohibitively large for numerical integration. However, if the coupling g is small, we can make the semiclassical approximation $\langle \hat{A}\hat{B} \rangle = \langle \hat{A} \rangle \langle \hat{B} \rangle$, thus neglecting all quantum correlations. This of course does not mean that the observables become uncorrelated in the classical sense! Classical correlations between observables will in fact become important in the following treatment of superradiance. Due to our specific choice of phase in the driving and dipole coupling terms, the equations for $\langle \dot{a} \rangle$ and $\langle \dot{a}^\dagger \rangle$ as well as $\langle \dot{J}_- \rangle$ and $\langle \dot{J}_+ \rangle$ are identical, which allows us to reduce the four equations to two real equations.

$$\langle \dot{a} \rangle = -\kappa \langle a \rangle + g \langle J_- \rangle + \eta \quad (2.61)$$

$$\langle \dot{J}_- \rangle = -(\gamma_{\parallel} + \gamma_{\perp}) \langle J_- \rangle + g \langle J_z \rangle \langle a \rangle \quad (2.62)$$

$$\langle \dot{J}_z \rangle = -2\gamma_{\parallel}(\langle J_z \rangle + 1) - 4g \langle J_- \rangle \langle a \rangle \quad (2.63)$$

This is an extended form of the the Maxwell-Bloch equations which includes the additional dephasing term γ_{\perp} . These equations are studied in many fields from Nuclear-Magnetic-Resonance (NMR) research over laser physics to optics.

In section 2.2.1 we discussed the Holstein-Primakoff approximation where one replaces the spin operators J_{\pm} with bosonic operators in the Hamiltonian. This approximation can also be done on the level of the equations of motion by setting $\langle J_z \rangle \equiv -N$, which also amounts to neglecting eq. (2.63). It is useful in the exploration of the low excitation regime and various extensions of the Maxwell-Bloch equations [39, 42].

2.4.1. Numerical Analysis for a Single Emitter

To understand the phenomenology behind the Maxwell-Bloch equations we first consider the case *without dissipation*, i.e. $\gamma_{\parallel} = 0$, $\gamma_{\perp} = 0$, $\kappa = 0$ and solve the equations numerically. Example solutions are plotted in fig. 2.4. It can be seen that the dynamics resemble those of a classical dipole. The upper panels show the case where a single emitter starts out in its ground state with less than one excitation in the bosonic mode, i.e. $\langle a(0) \rangle < 1$. The latter condition means that the emitter will never reach the fully excited state. The energy in the system oscillates between the bosonic mode and the emitter.

The lower panels of fig. 2.4 show the case where the number of bosonic excitations corresponds exactly with the number of emitters. After the emitter has absorbed the excitation from the bosonic mode it remains in the excited state just like a pendulum would, if one kicks it such that by the time it reaches the fully inverted position its kinetic energy becomes zero. This is a metastable state which becomes immediately obvious when one considers the form of the Maxwell-Bloch equations. In this state $\langle a \rangle = 0$ and $\langle J_- \rangle = 0$ which means that eq. (2.62) decouples completely from the emitter equations.¹

In fig. 2.5 another interesting feature is visible. If there is less than one excitation in the bosonic mode then the period of the oscillation increases with the mean number of excitations, becoming infinite for $n = 1$. Above this threshold the period decreases again. This is different from the dynamics of the full quantum mechanical Jaynes-Cummings model where for the case $n \leq 1$ the period of the oscillation is independent of n . For an initial state like

$$|\psi(0)\rangle = \frac{1}{\sqrt{A^2 + B^2}}(A|0\rangle + B|1\rangle)|\downarrow\rangle, \quad (2.64)$$

the time evolution is given by

$$|\psi(t)\rangle = \frac{1}{\sqrt{A^2 + B^2}} \left[A|0, \downarrow\rangle + B(\cos(gt)|1, \downarrow\rangle + \sin(gt)|0, \uparrow\rangle) \right]. \quad (2.65)$$

Next, we explore the effects of decoherence and decay on the dynamics. Figure 2.6 shows the dynamics in the presence of dephasing and bosonic mode decay

¹Due to the finite precision in a numerical simulation the metastable state will never be reached exactly, unless set as the initial state by hand. Therefore, an oscillation with a finite period will always be present.

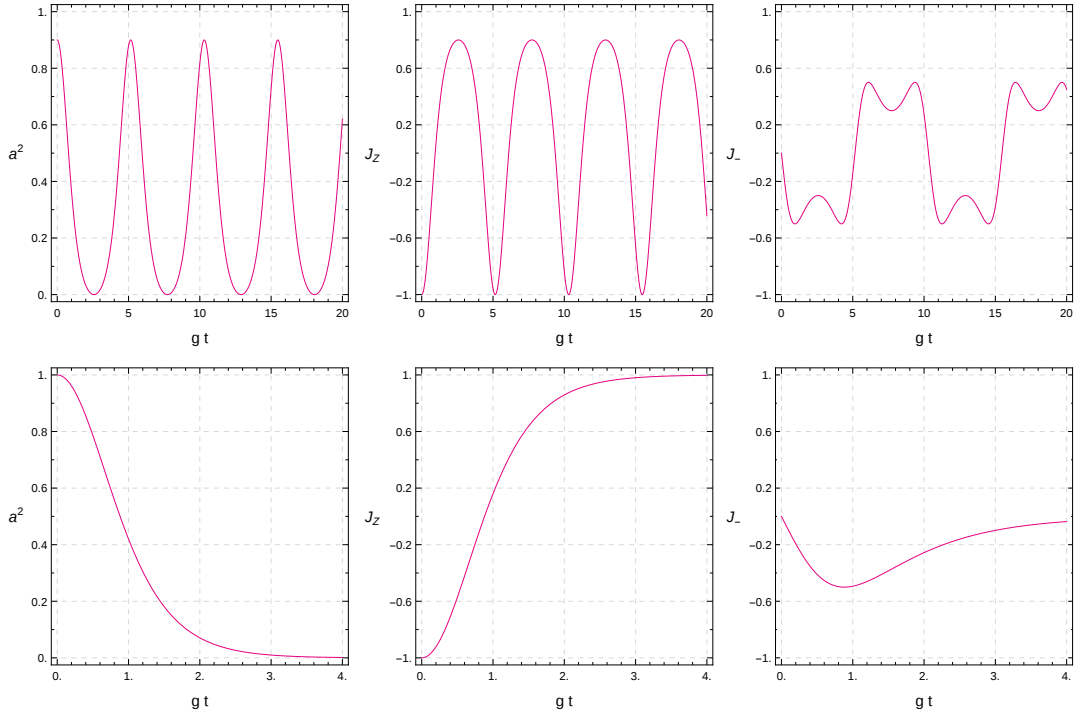


Figure 2.4.: Numerical solutions of the Maxwell-Bloch equations without dissipation ($\gamma_{\perp,\parallel} = 0$, $\kappa = 0$) in eqs. (2.62) to (2.63) for a single emitter in the ground state, i.e. $\langle J_z(0) \rangle = -1$, $\langle J_-(0) \rangle = 0$ and $\langle a(0) \rangle = \sqrt{0.9}$ (upper panels) as well as $\langle a \rangle = 1$ (lower panels).

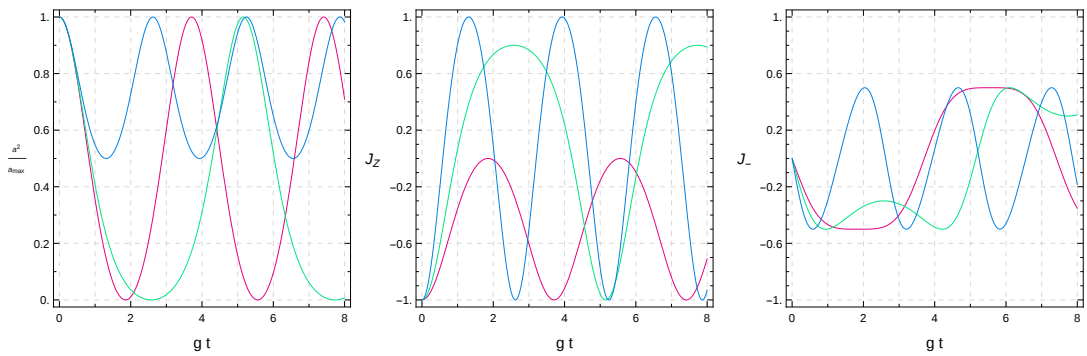


Figure 2.5.: Numerical solutions of the Maxwell-Bloch equations without dissipation ($\gamma_{\perp,\parallel} = 0$, $\kappa = 0$) in eqs. (2.62) to (2.63) for a single emitter in the ground state, i.e. $\langle J_z(0) \rangle = -1$, $\langle J_-(0) \rangle = 0$ and $\langle a(0) \rangle = \sqrt{0.5}$ (pink), $\langle a(0) \rangle = \sqrt{0.9}$ (green) and $\langle a(0) \rangle = \sqrt{2}$ (blue).

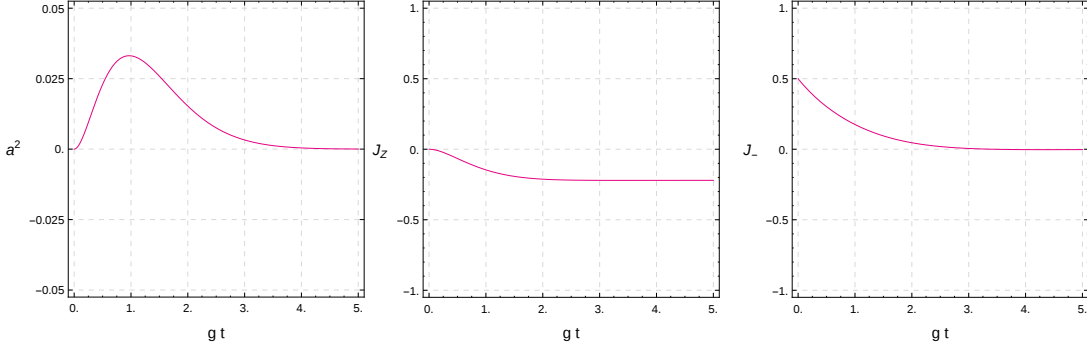


Figure 2.6.: Dynamics for a single emitter in a half excited initial state and no bosonic excitations $|\psi(0) = (1/\sqrt{2}) |0\rangle (|\uparrow\rangle + |\downarrow\rangle)\rangle$ with $g, \kappa, \gamma_{\perp} = 1$ and $\gamma_{\parallel} = 0$.

$\gamma_{\perp} = \kappa \neq 0$ but without emitter decay $\gamma_{\parallel} = 0$. When the initial state of the emitter contains some excitation and $g \approx \kappa, \gamma_{\perp}$, most of it gets trapped in the emitter because its polarization decays quicker than it can transfer the excitations to the bosonic mode. Note that the trapping will not happen if there is no cavity decay because the $\langle J_z \rangle \langle a \rangle$ term in the derivative of $\langle J_- \rangle$ will be non-zero and introduce small amounts of polarization that allow the transfer of excitations from the emitter to the bosonic mode.

More interesting features emerge when the drive term η is included. Figure 2.7 shows the dynamics with emitter dephasing and bosonic mode decay (the emitter decay γ_{\parallel} is set to 0). The excitations oscillate between the bosonic mode and the emitter till $\langle a \rangle$ and $\langle J_- \rangle$ reach a steady state. But the emitter continues to absorb excitations that are pumped into the system by the drive, i.e. $\langle J_z \rangle$ increases. A steady state will eventually be reached as soon as $\langle J_z \rangle$ becomes 0 which will force $\langle J_- \rangle$ to become 0 too.

This case is shown in the upper panels of fig. 2.8. As soon as $\langle J_z \rangle$ reaches 0, oscillations set in again. This can be analyzed by linearizing the Maxwell-Bloch equations around that steady state. Lastly we add emitter decay γ_{\parallel} to the analysis and see that we obtain an additional steady state where both $\langle J_z \rangle$ and $\langle J_- \rangle$ are non-zero. When the drive is turned off, this leads to oscillations since the emitter can again release its excitations into the bosonic mode without being reexcited by the drive.

For the case where all emitter dephasing and decay channels are zero, i.e. $\gamma_{\perp} = 0$ and $\gamma_{\parallel} = 0$, there are three cases that can be distinguished. They are discussed in [41, Chapter 16.3.1] in great detail and are mentioned here briefly for completeness. The three cases are classified by $\eta/g < 1/2$, $\eta/g = 1/2$ and $\eta/g > 1/2$. In the first case the emitter polarization cancels the drive, i.e. the emitter destructively interferes with the driving field. Since there are no dephasing and decay channels a finite polarization of the emitter also implies a finite excitation. The bosonic mode on the other hand decays to 0. In the second case the emitter

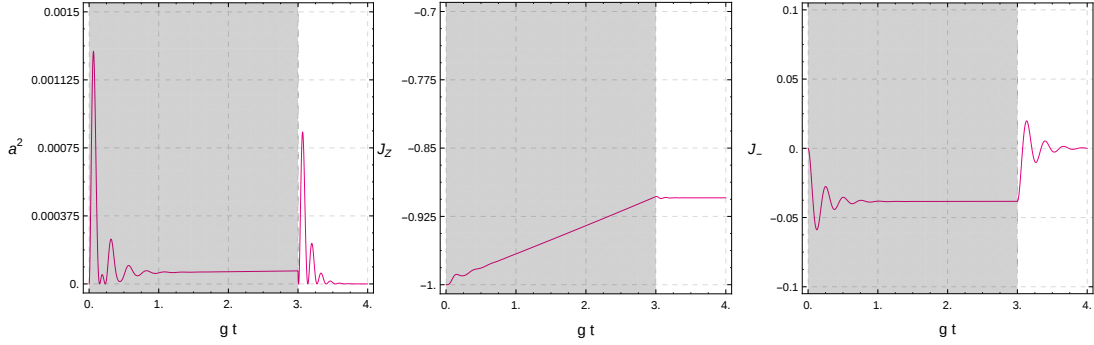


Figure 2.7.: Dynamics of a single emitter for $\gamma_{\perp} = \kappa = 1$, $\gamma_{\parallel} = 0$ and $g = 5$. The shaded area shows the period of time when the drive term η is set to 0.2.

polarization reaches its maximum and barely cancels the drive. This drive is called the critical drive. In the last case the emitter can not fully cancel the external field which leads to oscillations.

The effects of additional emitters will be discussed at the end of the next section, after the phenomenon of superradiance has been introduced.

2.5. Superradiance - Coherent Spontaneous Emission

2.5.1. Dicke's Thought Experiment

In the previous sections we have introduced the necessary tools and models to study the main topic of this thesis - superradiance. This phenomenon was first described by Dicke in 1964 [1]. He considered a dipole coupled emitter - emitter A - initialized in its excited state. Such an emitter will spontaneously decay to its ground state. If we introduce a second emitter - lets call it B - in its ground state, the wave function of the combined system will be the product of the individual wave functions. It is furthermore assumed that the emitters are far enough apart so that the symmetry properties of the total wave function do not have to be considered. This product wave function can be expressed as a superposition of a singlet and triplet state

$$|\psi\rangle = |\uparrow, \downarrow\rangle = \frac{1}{2}(|\uparrow, \downarrow\rangle + |\downarrow, \uparrow\rangle) + \frac{1}{2}(|\uparrow, \downarrow\rangle - |\downarrow, \uparrow\rangle). \quad (2.66)$$

The dipole operator for the whole system is given by

$$d = (\sigma_A^- + e^{ikr_{AB}} \sigma_B^-) + (\sigma_A^+ + e^{-ikr_{AB}} \sigma_B^+). \quad (2.67)$$

If the distance between the two emitters r_{AB} is small compared to the wavelength that corresponds to the energy difference between the excited and ground states,

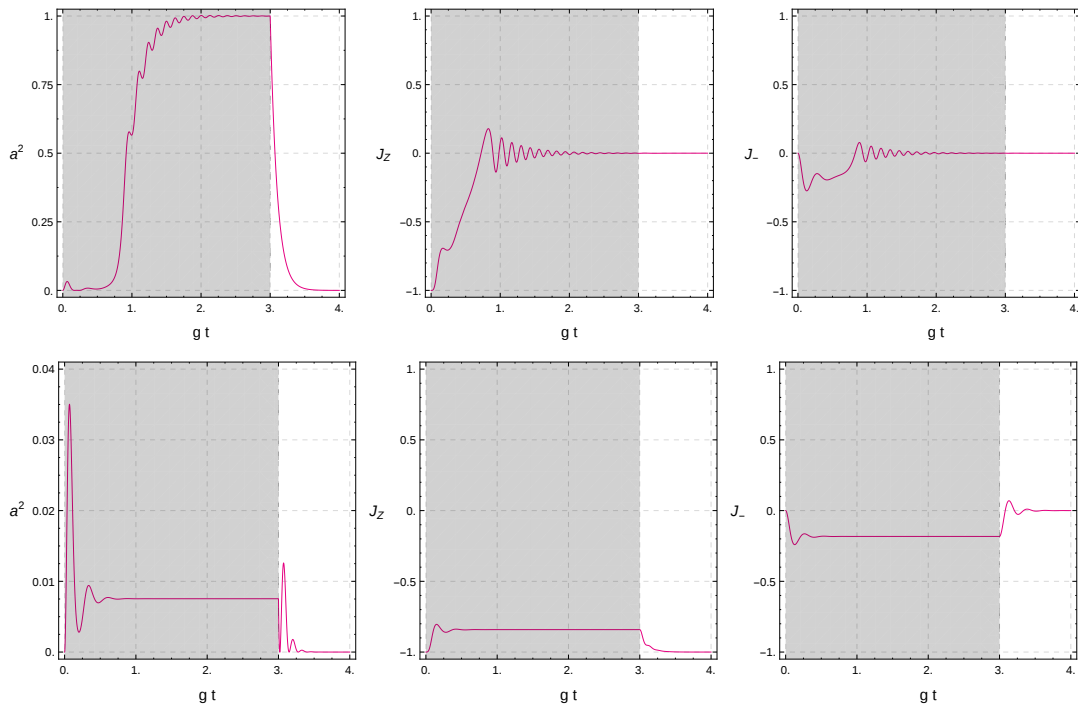


Figure 2.8.: Dynamics of a single emitter for $\gamma_{\perp} = \kappa = 1$, $\gamma_{\parallel} = 0$ and $g = 5$. The shaded area shows the period of time when the drive term η is set to 1. The upper panels show the case without emitter decay $\gamma_{\parallel} = 0$ and the lower panels the case with $\gamma_{\parallel} = 1$. Note that for sufficiently high drive terms η the lower panels would look similar to the upper ones.

then we can set the phase factor to 1. This is the case that Dicke considered in his thought experiment. In this case the dipole moment of the singlet part of the wave function becomes 0 which prevents this part of the wave function from decaying. This is very similar to classical interference of electromagnetic fields which is dependent on the phase relation of the emitters. However, while for classical dipoles the phase can only be encoded in the temporal or spatial domain, there is also the phase of the wave function in the quantum case.

The triplet part will decay exponentially on a timescale t_t that can be computed with Fermi's Golden rule. But this will only lead us to the probability of decay *conditional* on the system being in the triplet state. The probability of finding both emitters in their ground states for $t \gg t_t$ is $1/2$, because this is the probability to find the system in the triplet state. This is very different from the case without emitter B, where the probability of finding emitter A in its ground state would reach 1. We also note that if the emitters were prepared in the triplet state, both would reach the ground state with absolute certainty and do so at a rate that is twice as large as the spontaneous emission rate for a single emitter.

2.5.2. Coherence

Dicke used the above example to illustrate the importance of interference phenomena and therefore coherence, for the spontaneous emission process. Coherence for classical emitters means that their emitted radiation has a constant phase relation. Ideally one wants all emitters to have exactly the same phase so that their emitted fields can constructively interfere. Assuming that we have N waves with unit amplitudes and phases $\phi_i \in [0, 2\pi]$ propagating in one dimension, the intensity at some point in space at time t is given by

$$\begin{aligned}
 I(t) &= \sum_{i,j}^N \cos(\omega t + \phi_i) \cos(\omega t + \phi_j) \\
 &= \sum_i^N \cos(\omega t + \phi_i)^2 + \sum_{i \neq j}^N \cos(\omega t + \phi_i) \cos(\omega t + \phi_j).
 \end{aligned} \tag{2.68}$$

If the waves have random phases, i.e. if they were emitted incoherently, the second term is going to average to 0 and thus the intensity will scale with N . In the case of coherent radiation - where all phases are equal - the second term is not zero and the intensity scales with N^2 . For quantum emitters, separated by a distance smaller than the wavelength, a difference in phase can either emerge through the phases within the collective wave function, like in Dicke's thought experiment, or through a difference in the time evolution of their respective wave functions. If the wave function is symmetric under emitter permutation, then all emitters must have the same phase. If the wave function has this symmetry for all times then the phase due to the time evolution is also equal. Therefore, if the

permutation symmetry condition is fulfilled for all times, the emission process is coherent.

The states that are symmetric under emitter permutations are those that share excitations equally among all emitters. We can obtain these states by starting in the state where all emitters are excited and apply the collective ladder operator as defined in eq. (1.4). The initial state clearly fulfills the symmetry requirement and has the highest number of excitations while the ladder operator can not break the symmetry since it is itself symmetric. In this way we can generate all fully symmetric states labeled by the number of excitations. The normalized states are given by [43, Equation 2.6]

$$|j, m\rangle = \sqrt{\frac{(j+m)!}{N!(j-m)!}} \left(\frac{1}{2} \sum_i^N \sigma_i^- \right)^{j-m} |\uparrow, \uparrow, \dots, \uparrow\rangle. \quad (2.69)$$

With $j = N/2$ and $-j \leq m \leq j$ where N denotes the number of emitters. In the context of superradiance these states are usually referred to as Dicke states, but they are identical to angular momentum eigenstates. That means that the conversion between the individual and the symmetric basis could also have been done through the Clebsch-Gordan formalism. The initial state corresponds to $|j, m = j\rangle$ and the ladder operator is just the same as in the angular momentum formalism. Importantly, any superposition of these states will also be symmetric under emitter permutation. While each of these states features entanglement among the emitters there are superpositions that do not. For example, the product states

$$|\psi_\theta\rangle = \prod_{i=1}^N (\cos(\theta) |\uparrow\rangle_i + \sin(\theta) |\downarrow\rangle_i), \quad (2.70)$$

can be expressed as superpositions of $|j, m\rangle$ with j fixed to $N/2$. One way to see that this is true is to observe that any set of $|j, m\rangle$ states with a fixed j forms a complete basis for a subspace of the Hilbert space of the corresponding symmetry. Another way to see this is to consider the Hamiltonian that describes a single emitter that is coherently driven by a classical field with amplitude η

$$H = \frac{\hbar\omega}{2} \sum_i \sigma_i^z + \hbar g \sum_i (\sigma_i^+ e^{-i\omega t} + \sigma_i^- e^{i\omega t}) = \frac{\hbar\omega}{2} J_z + \hbar g \eta (J_+ e^{-i\omega t} + J_- e^{i\omega t}). \quad (2.71)$$

The solution is given by the time dependent spin coherent states with $\theta = gt$. As the collective operator notation suggests, the time evolution due to this Hamiltonian always stays within a subspace that is spanned by the $|j, m\rangle$ states. As will be shown in the next section, the intensity of radiation in this case can be computed with

$$I = I_0 \langle J_+ J_- \rangle = I_0 \left(\sum_i^N \langle \sigma_i^+ \sigma_i^- \rangle + \sum_{i \neq j}^N \langle \sigma_i^+ \sigma_j^- \rangle \right). \quad (2.72)$$

For a spin coherent state the second term will not be zero which means that the intensity will still scale with N^2 . We went through this exercise to demonstrate that the entanglement of the triplet state in Dicke's thought experiment is not a necessary condition for coherence.

2.5.3. Superradiance in Vacuum

In his original work Dicke considered an ensemble of dipoles that is coupled to a vacuum mode. In the formalism of the master equation that corresponds to an environment that consists of a *single oscillator* at zero temperature, i.e. an environment that can absorb radiation with momentum vectors in all possible directions but only of one particular energy.² We know that the operators J_{\pm} are the ones that enter the dipole coupling and thus couple the system to the environment. Therefore, the only thing that we need to do is plug them into the Lindblat master equation that we derived in eq. (2.41). The Hamiltonian of the ensemble is given by $H = \frac{\hbar\omega}{2} J_z$, but it will be omitted in the following because we will be working in the rotating frame. We obtain the superradiance master equation

$$\dot{\rho} = \frac{\gamma_{\parallel}}{2} (2J_- \rho J_+ - J_+ J_- \rho - \rho J_+ J_-), \quad (2.73)$$

where γ_{\parallel} corresponds to the single emitter decay rate. The amazing insight of Dicke was that due to the collective coupling to the environment the system will not leave the symmetric subspace of the initial state and therefore feature coherence effects. Note that the above equation is very different from

$$\dot{\rho} = \frac{\gamma_{\parallel}}{2} \sum_i^N (2\sigma_{-i} \rho \sigma_{+i} - \sigma_{+i} \sigma_{-i} \rho - \rho \sigma_{+i} \sigma_{-i}), \quad (2.74)$$

where there are no coherence effects and each emitter is damped independently of the rest. Because of the preserved symmetry it makes sense to express the above equation in the $|j, m\rangle$ basis. Furthermore, we note that the off-diagonal terms of the density matrix are not coupled to the diagonal ones. The superradiance master equation for the diagonal terms of the density matrix in the $|j, m\rangle$ basis is

$$\dot{\rho}_m = -\gamma_{\parallel} (j+m)(j-m+1)\rho_m + \gamma_{\parallel} (j+m+1)(j-m)\rho_{m+1}, \quad (2.75)$$

where ρ_m represents the probability of finding the system in state $|j, m\rangle$. There are $2j+1$, if j is a half-integer, or $2j$ of these equations, if j is an integer. They can be numerically integrated for small j . In [43] an overview over approximate results is provided and in [44, 45] the exact solution for the master equation as well as a few useful expectation values are obtained. The corresponding equations

²If we drop this requirement the effects of dipole-dipole interactions between the emitters become relevant [43].

of motion are

$$\langle \dot{J}_z \rangle = -2\gamma \langle J_+ J_- \rangle, \quad (2.76)$$

$$\langle \dot{J}_- \rangle = \frac{\gamma}{2} \langle J_z J_- \rangle. \quad (2.77)$$

Because of energy conservation $\langle \dot{J}_z \rangle = \langle \dot{n} \rangle$, with $n = a^\dagger a$. Therefore, the first equation can be rewritten to an equation for the cavity amplitude. For brevity we will not deal with these solutions here but only present the most important properties of superradiance, following [43].

One doesn't need to solve the full master equation to make some interesting observations. We can think of superradiance as a cascade down the ladder of Dicke states. Each step is considered as an independent spontaneous emission process of one excitation. The rate of emission for the $(j - m - 1)$ th photon is

$$\Gamma_{m \rightarrow m-1} = \gamma_{\parallel} |\langle j, m-1 | J_- | j, m \rangle|^2 = \gamma(j+m)(j-m+1). \quad (2.78)$$

Here γ_{\parallel} denotes the spontaneous emission rate of a single excited emitter. A term that is identical to the right hand side of this equation also appears in the master equation. However, while Fermi's golden rule gives us a transition probability the term in the master equation should rather be interpreted as a coupling. Both concepts are similar but not identical to each other. We see that for $m = 0$ the term scales with j^2 and thus with $(N/2)^2$ just as we would expect for a coherent process. This maximal rate is only reached if there is a point in time when the system is *completely* in the $|j, m = 0\rangle$ state. For a general state, that is symmetric under emitter permutations, the rate of photon emission is given by

$$\Gamma_{total} = \sum_{m=-j}^j p_m \gamma_{\parallel} (j+m)(j-m+1), \quad (2.79)$$

where p_m denotes the probability of being in the state $|j, m\rangle$. We can approximate the rate at which the $s = (j - m)$ th photon is emitted with $\Gamma_s = \gamma_{\parallel} N s$. Since we assumed that the emissions are independent we can obtain the average time $\langle t_d \rangle$ (the brackets denote an average over multiple trials, not a quantum mechanical average) that it would take to reach the $|j, m = 0\rangle$ state by summing the average times of each individual photon emission

$$\langle t_d \rangle = \sum_{s=1}^{N/2} \frac{1}{\Gamma_s} = \frac{1}{N\gamma_{\parallel}} \sum_{s=1}^{N/2} \frac{1}{s} \approx \frac{\log(N/2)}{N\gamma_{\parallel}}. \quad (2.80)$$

We see that the timescale of independent spontaneous emission $\langle t_{ind} \rangle = 1/\gamma_{\parallel}$ is significantly reduced. In incoherent spontaneous emission the rate is constant over time while in superradiant decay the rate grows till the $N/2$ th photon is

emitted. To obtain the incoherent case from the superradiant one, we can introduce random phases $\phi_i \in [0, 2\pi]$ in the collective ladder operator

$$J_-^{incoh} = \sum_{i=1}^N e^{i\phi_i} \sigma_i^- . \quad (2.81)$$

Plugging this in eq. (2.78) and omitting the interference terms (which become 0 because of the random phases) we obtain

$$\Gamma_{incoh} = \gamma_{\parallel} \sum_{i=1}^N |\langle \downarrow|_i \sigma_-^i |\uparrow\rangle_i|^2 \quad (2.82)$$

In the incoherent case we know that a particular spin has decayed if we detect a photon. I.e. if we were able to identify this emitter, the consequent dynamics would not change. In the superradiant case each emitter contributes $1/N$ th of the emitted photon. If we were to stop the dynamics and measure each emitter to determine which one has decayed, we would break the permutation symmetry and alter the consequent dynamics considerably.

It should be noted that each photon emission is a stochastic process and that the system can emit multiple photons at once. Therefore, the above picture of the system falling from one rung of the Dicke ladder to the next is inaccurate. With this picture in mind one might expect that the wave function of the system can be described by a superposition of Dicke states $|j, m\rangle$ at all times or that the wave function even corresponds to the Dicke states at certain times which would also mean that the emitters become entangled in the process. However, both statements are incorrect. Since the master equation does not couple diagonal terms to the off-diagonal ones the density matrix remains diagonal during the process and since the diagonal entries become smaller than one $Tr(\rho^2) = \sum_m^N p_m^2 < 1$ because $p_m < 1$ for all m , which means that the state becomes mixed. This is of course just the same as in the case of regular spontaneous emission.

In the vacuum case the time evolution is dependent on $\langle J_+ J_- \rangle$ while in the case of Hamiltonian dynamics with the semiclassical approximation it is only dependent on $\langle J_- \rangle$ as is evident from the Maxwell-Bloch equations in eqs. (2.62) to (2.63). Note that the expectation value $\langle J_+ J_- \rangle$ can not be factorized into $\langle J_+ \rangle \langle J_- \rangle$ because the operators J_+ and J_- do not commute. J_- and a^\dagger on the other hand operate on different Hilbert spaces and the expectation value of their product can be factorized if the coupling between the two Hilbert spaces is small.

The fact that $\langle J_+ J_- \rangle$ can not be factorized means that one can not derive this result directly from the Maxwell-Bloch equations in eqs. (2.62) to (2.63) by assuming $\kappa \gg g$ and eliminating the equation for the cavity amplitude. Instead, the cavity amplitude must be eliminated on the level of operator equations and the expectation values must be taken afterwards. It is this change that makes superradiance in vacuum so different than in the presence of a cavity mode. In the prior case, coherence emerges spontaneously and is thus completely stored

in the emitter ensemble while in the latter case coherence emerges through the interaction with a common field. Furthermore, if a weakly coupled cavity mode is present then dephasing can lead to $\langle J_- \rangle = 0$, thus highly suppressing the decay of the emitter ensemble. This is different in the vacuum case as can be seen from eq. (2.76) and eq. (2.82).

So far we have considered an ensemble of emitters in vacuum where there is no feedback from the emitted photons back onto the ensemble because the photons immediately disappear. This is quite different from the closed-system models that were presented in earlier sections, where the photons keep interacting with the ensemble which leads to stimulated emission. Another difference is that in the absence of decay channels the system remains in a pure state. To study these cases we turn again to the Maxwell-Bloch equations from eqs. (2.62) to (2.63). Without decay these equations are equivalent to those that describe the dynamics of a classical dipole as is shown in [7, Section III]. Therefore, we first look at these dynamics from a purely classical point of view before we turn to numerical solutions of the Maxwell-Bloch equations for multiple emitters.

2.5.4. Classical Aspects of Superradiance

A classical dipole in an external field experiences the torque

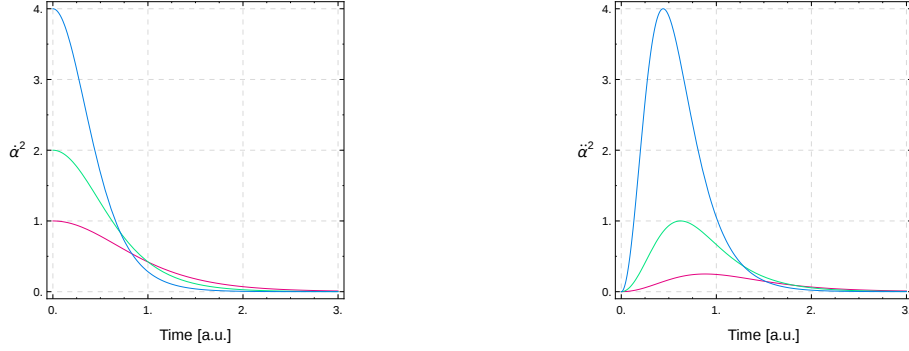
$$\boldsymbol{\tau} = \boldsymbol{\mu} \times \mathbf{B}. \quad (2.83)$$

While we choose the usual notation for magnetic dipoles the following applies to electric dipoles as well unless explicitly stated otherwise. If the dipole is not aligned exactly parallel or antiparallel with the external field, it will start rotating in the direction of the external field. Losing its potential energy and gaining kinetic energy. As is evident from eq. (2.83) the torque will be time dependent because the angle between $\boldsymbol{\mu}$ and \mathbf{B} will change in time. However, to determine the dynamics we have to specify more details about the physical system. We can imagine the dipole to be a bar magnet that is initially at rest. It has a certain moment of inertia I and no angular momentum at the beginning.³

³Since magnetic moments of spins are always associated with an angular momentum the bar magnet actually does have a finite angular momentum even if it is at rest. Therefore, we might expect that a bar magnet precesses in a static magnetic field just like a spinning top would in a gravitational field. The relation between the angular momentum and the magnetic moment is given by

$$\boldsymbol{\mu} = g \frac{-e}{2m_e} \mathbf{L} = \frac{g\mu_B}{\hbar} \mathbf{L} = \gamma \mathbf{L}. \quad (2.84)$$

The gyro-magnetic ratio in this case is $\gamma = 1.76 \cdot 10^{11} (\text{sT})^{-1}$. This means that the angular momentum is negligibly small compared to the torque and the moment of inertia of the structure. Note however that this argument does not apply to the quantum mechanical spins themselves. Since the precession of a quantum mechanical spin happens on the level of the wave function and does not involve moving around any mass, a quantum mechanical spin will always precess in a static external field no matter how small.



(a) The square of the function in eq. (2.87). (b) Square of the first derivative of eq. (2.87).

Figure 2.9.: Solutions for the equations of motion of a classical pendulum for $J = 1$, $J = 2$ and $J = 4$.

The Lagrangian of this system is

$$\mathcal{L}(\alpha, \dot{\alpha}) = E_{rot} - E_{pot} = \frac{1}{2}I\dot{\alpha}^2 - \mu B \cos \alpha, \quad (2.85)$$

with α denoting the angle between the external field axis and the dipole direction. This leads us to the following equation of motion

$$\ddot{\alpha} = \frac{\mu B}{I} \sin(\alpha) = J \sin(\alpha). \quad (2.86)$$

This equation is equivalent to the equation of motion of a pendulum (without the small angle approximation), which can be analytically solved [46]. It has a metastable solution $\alpha(0) = 0$, $\dot{\alpha}(0) = 0$. Any small deviation from this state leads to a time dependent, periodic solution. The size of the deviation determines the period of the oscillation. In the limit $\alpha(0) \rightarrow 0$ and $\dot{\alpha}(0) \rightarrow 0$ the period becomes infinite. In this case the solution is given by [7, 47]

$$\dot{\alpha}(t) = 2\sqrt{J}\operatorname{sech}\left(\sqrt{J}t\right). \quad (2.87)$$

This solution assumes that the dipole starts in its metastable state $\alpha = 0$ at $t = -\infty$. The square of this function and the square of its derivative are plotted in fig. 2.9. We see that $\dot{\alpha}^2(t)$ scales with J , while $\ddot{\alpha}^2(t)$ scales with $(J/2)^2$. As we can guess from fig. 2.9a the dipole is parallel with the field at $t = 0$ because its angular velocity is maximal at this time. The square of the angular velocity enters the rotational energy. However, while the velocity is dependent on the ratio of the dipole moment to the moment of inertia, the rotational energy is dependent on the dipole moment alone, i.e. it scales with μ . Same goes for the first derivative of the rotational energy.

How do the dynamics change if we had two of such dipoles next to each other? Each of them will rotate in exactly the same way as when the other one was not there but the total rotational energy will be twice as large. Everything will remain exactly the same if we were to replace the two separated dipoles with a single one whose dipole moment and moment of inertia are twice as large.

We see that increasing the number of classical dipoles doesn't change the dynamics, no matter how they are arranged. We can only change the dynamics if we change the dipole moment while keeping the moment of inertia constant. In the previous example of a bar magnet we would have to change the strength of a ferromagnet.

We have established that for classical dipoles the rotational energy scales with the size of the dipole moment while the change in rotational energy scales with the square of the dipole moment if everything else is kept constant. While the equations of motion are identical to the equations of motion for the quantum mechanical system in the rotating frame, the dipole moment is a classical vector quantity and its absolute size can not change due to interference effects. However, in interacting classical systems the growth and decay of the total dipole moment in time, analogous to the interference in the quantum mechanical systems, is known [48].

2.5.5. Maxwell-Bloch Equations for Multiple Emitters

In the case of quantum mechanical dipoles we expect very similar dynamics as in the classical case discussed above. Additionally we will look at how the dephasing and decay channels as well as the drive term affect these dynamics.

In fig. 2.10 we plot numerical solutions for the cases of $N = 1, 2, 4$ emitters with the initial excitation of the bosonic mode corresponding to the number of emitters in each case $\langle a^\dagger a \rangle = \langle a \rangle^2 = N$. We see that an increase in the number of emitters leads to an increase in the absorption rate of the bosonic excitations by the emitters. If we imagine the bosonic mode to be a bucket of water then the number of emitters could correspond to the number of holes through which water can escape. The same amount of water would escape quicker if there were more holes. However, if we increase the amount of water by the same factor as we increase the number of holes then the time it would take to empty the bucket completely, would remain constant. The dynamics that we observe here is different: even though the number of excitations has increased by the same factor as the number of emitters the time till all of them are absorbed decreased. One can say that the exchange of excitations between the bosonic mode and the emitters happens non-linearly.

How can this scaling be explained? We can not resort to the previously used argument of an increasing transition amplitude that we obtained from Fermi's Golden rule, because a transition amplitude does not appear in the Maxwell-Bloch equations. The coupling between the emitters and the field is governed by

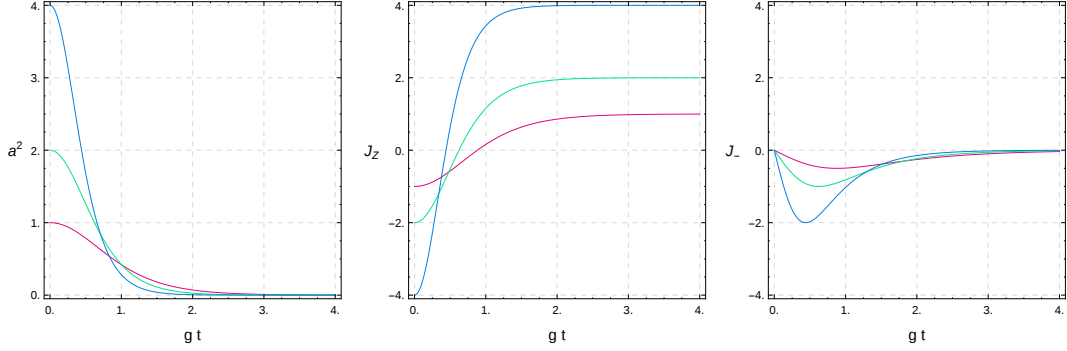


Figure 2.10.: Numerical solutions to the Maxwell-Bloch equations without dissipation ($\gamma_{\perp,\parallel} = 0$, $\kappa = 0$) in eqs. (2.62) to (2.63) for 1 (pink), 2 (green) and 4 (blue) emitters in the ground state, i.e. $\langle J_z(0) \rangle = -1, -2, -4$, $\langle J_-(0) \rangle = 0$ and $\langle a(0) \rangle = 1, \sqrt{2}, \sqrt{4}$.

$\langle J_- \rangle$. We also made the semiclassical approximation which amounts to neglecting the quantum correlations between the bosonic mode and the emitters. From the point of view of the wave function this corresponds to the assumption that the total wave function is a product of the bosonic and the emitter part. Since the Maxwell-Bloch equations do not contain interaction terms between the emitters, the emitter part of the wave function must be a product state of individual emitter wave functions. Because of the symmetric coupling of all emitters the total wave function must be symmetric under emitter permutations.

The most general state that fulfills these conditions is a product state of the bosonic coherent state and the spin coherent state

$$|\psi(t)\rangle = |\alpha(t)\rangle \prod_{i=1}^N (\cos(\theta(\alpha)t) |\downarrow\rangle_i + \sin(\theta(\alpha)t) |\uparrow\rangle_i). \quad (2.88)$$

This is arguably the most classical state of this quantum system. Its properties are identical to the states that are generated by exposing an ensemble of two-level systems to a classical driving field. In this case the driving field is the coherent state of the bosonic mode. Therefore the time evolution of the emitter state is coupled to the state of the bosonic mode. This is why θ depends on α in the above equation.

The reason for the seemingly increased absorption is that there is a larger external field to drive the emitters. The solutions plotted in fig. 2.10 are identical to eq. (2.87). There we see the $\sqrt{J} = \sqrt{N}$ dependence of the timescale which in this case translates to the square root of the number of bosonic excitations because we have chosen the initial condition such that the number of excitations corresponds to the number of emitters. Starting in the state $\langle J_z \rangle = N$ and $\langle a \rangle = 0$ would lead to the same \sqrt{N} scaling because the rate at which the number of excitations would increase in the bosonic mode is higher when more emitters are

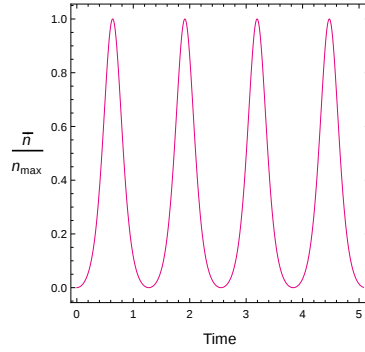


Figure 2.11.: Mean photon number as derived in [7]. This is a plot of eq. (2.90) for $j = 10$, $m = 10$, $a = \ln(4)$.

present. This higher field would in turn stimulate the emitters to transfer their excitations even faster into the bosonic mode leading to a non-linear behavior.

The hallmark sign of coherence and superradiance is the N^2 scaling. Looking at the Maxwell-Bloch equation for the bosonic mode in eq. (2.62), which we reproduce here (without the driving term),

$$\langle \dot{a} \rangle = -\kappa \langle a \rangle + g \langle J_- \rangle, \quad (2.89)$$

we see that the derivative of $\langle a \rangle$ is proportional to $\langle J_- \rangle$ which is in turn proportional to N . Thus, in the case of Maxwell-Bloch equations the characteristic scaling emerges in the first derivative of the field. In vacuum, however, the field decays so quickly that it is directly proportional to its derivative. It should be noted that the non-linearity discussed here is equivalent to the non-linearity of a classical pendulum. Furthermore, as can be seen from eq. (2.89) the scaling with the number of emitters is equivalent to a scaling of the coupling g . Therefore, neither the non-linearity nor its scaling are dependent on the presence of *multiple* emitters.

In this section we have discussed the phenomenon of superradiance in the semiclassical approximation. However, it should be noted that the metastable state of these equations is unphysical. Quantum fluctuations lead to spontaneous emission and thus prevent the fully inverted state from being metastable. The implementation of these fluctuations into the semiclassical solution was done in [7]. They find that the *mean number* of excitations in the bosonic mode is given by

$$\bar{n}(t) = (j + m) \text{cn}^2[(2j + 1)^2(t - T)|k], \quad (2.90)$$

where cn denotes the Jacobi elliptic function, $k = (j + m)/(2j + 1)$ and $T = (2j + 1)^{-1/2}[a - \ln(1 - k)/2]$ with $\ln(4) \leq a \leq \pi/2$. This solution is plotted in fig. 2.11.

3. Experimental System

The quantum optics phenomena that were discussed in the previous chapter can be observed in many experimental setups [49, 50]. For the experimental part of this thesis we used an ensemble of Nitrogen-Vacancy (NV^-) defect centers in a diamond as the ensemble of emitters. Its properties will be introduced in the following section. The diamond was placed inside of a 3D cavity which constituted the bosonic mode and will be described in section 3.2. To initialize the NV^- ensemble in its ground state the cavity and the diamond were cooled down to 25mK in a dilution refrigerator. This also helped to decouple the ensemble from noise photons, as well as reduced lattice vibrations of the diamond and reduced cavity losses.

3.1. The Nitrogen Vacancy Defect Center in Diamond

The NV^- lattice defect has remarkable properties that make it a promising contender for quantum information processing and communication. One of the applications in quantum information processing is the quantum memory, there the NV^- center is not used directly but rather serves as a means to address the C^{13} nuclear spin that has a coherence time in the range of seconds [31]. The NV^- center can be used in transducer nodes in quantum communication networks [51] and was recently used in the first loophole-free Bell test [52, 53]. Beside its comparatively long life- and decoherence times the NV^- center can also be optically addressed, initialized and read-out. It is sensitive to external fields, stress and temperature which makes it useful for quantum metrology applications. Since diamonds are bio-compatible it can also be used as a marker for in vivo imaging of biological samples. Another very promising diamond-defect for quantum information processing is the silicon-vacancy center (SiV). It has even better coherence properties than the NV^- center because of higher symmetries [54]. However, its applications for metrology are limited. Diamonds have a multitude of other defects ("color centers") which have been known for many years because they affect the color of diamonds.

Diamonds consist of covalently bonded carbon atoms that are arranged in two inter-penetrating face-centered cubic (fcc) lattices. The diamond lattice is extremely rigid and has the widest optical transparency band of all known solids. This facilitates the detection of optically active defects and impurities. The

most abundant ones are typically nitrogen, boron, hydrogen, nickel, silicon and phosphorous.

In our experiments we used synthetic high pressure high temperature (HPHT) diamonds of the 1b type. These diamonds usually have a yellow or brown tone and the dominating defect in them is the P1 center. It consists of a nitrogen atom that forms four bonds with the neighboring carbon atoms. Since nitrogen has five valence electrons one remains unpaired and causes the paramagnetic nature of the defect with $S = 1/2$ and $g \approx 2$ [55]. Typical concentrations of nitrogen in type 1b diamonds range from 10^{17} cm^{-3} to 10^{19} cm^{-3} . Concentrations are often stated in parts-per-million (ppm) with $1 \text{ ppm} = 1.76 \times 10^{17} \text{ cm}^{-3}$ for diamonds.

The NV^- defect is formed if there is one empty lattice site next to a nitrogen atom and the other three are occupied by carbon atoms. The nitrogen can either be naturally present in the lattice or implanted in a controlled way. The diamond is then irradiated with electrons or neutrons to create lattice vacancies. These vacancies become mobile when the diamond is heated above 650°C . When a vacancy arrives at a lattice site next to a nitrogen atom it becomes trapped again and forms the NV^- center. Details about the preparation of the samples can be found in [56]. Since the center consists of two lattice sites it has a definite direction as can be seen in fig. 3.1. Therefore, a diamond will have four different subensembles of NV^- centers with different orientations.

The defect consists of six electrons in total [57]. Three from the dangling bonds of carbon atoms at the vacant lattice site and two from the nitrogen atom. The sixth electron is captured from the lattice giving the defect its negative charge. Only 2% of the electron density is found at the nitrogen atom. The configuration where no additional electron is captured from the lattice is also stable and is referred to as the NV^0 center.

3.1.1. Level Structure

The level structure of the ground and the first excited state is depicted in fig. 3.1. It was found that the NV^- ground state is a paramagnetic spin triplet state. The ground state features a zero-field-splitting (ZFS, marked with D in fig. 3.1), i.e. it is non-degenerate even if no external magnetic field is applied. The ZFS emerges because of interactions between unpaired electrons. This makes it very suitable for various applications because no strong external fields are needed to separate the states. The ZFS is also dependent on temperature and strain making the NV^- defect useful for quantum metrology. To be able to exploit quantum effects in metrology and other applications, a well defined quantum state needs to be prepared. For the NV^- center this can conveniently be done through the optically induced spin polarization mechanism [58] which enables the initialization of the NV^- center in its $m = 0$ ground state at room temperature.

For the experiments in this thesis it was necessary to initialize the whole ensemble of NV^- centers in its ground state. So far there exists no experimental

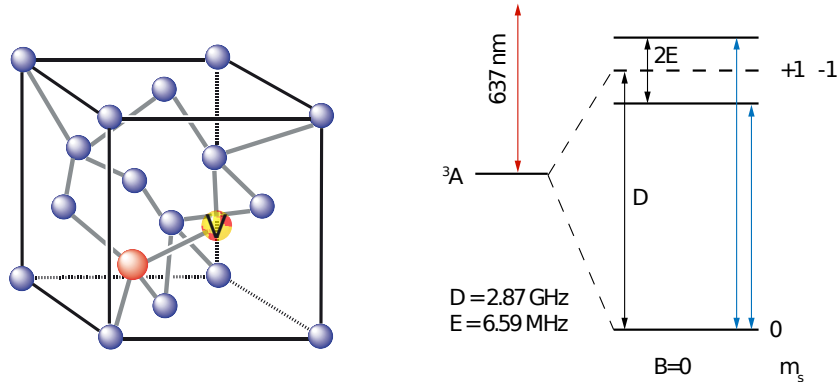


Figure 3.1.: Structure of the NV^- center consisting of a nitrogen atom and an adjacent vacancy (left). Energy levels of the ground state (right).

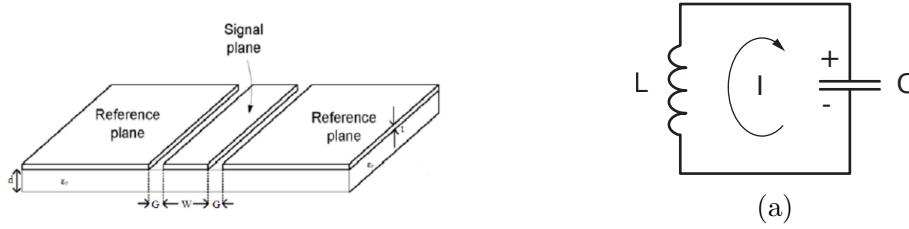


Figure 3.2.: A schematic of a coplanar waveguide (left). An LC circuit diagram (right).

evidence that the optically induced spin polarization mechanism can be used for this purpose. Instead, the NV^- ensemble was polarized thermally by cooling the diamond to 25mK inside of a dilution refrigerator.

3.2. 3D Cavity

A range of experiments have been performed with NV^- centers coupled to a superconducting coplanar waveguide (CPW) cavity [59]. These structures were developed to couple superconducting qubits for quantum information processing [60]. The advantage of the CPWs lies in the fact that the mode volume is a lot smaller than the wavelength which strongly increases the field that is produced by a single excitation of the superconducting wire. The coupling to an electronic spin is given by

$$g = \frac{\mu_B g_e}{\hbar} \sqrt{\frac{\mu_0 \hbar \omega}{2V}}, \quad (3.1)$$

which immediately follows from the form of the magnetic dipole coupling and the quantization of the cavity field. But how can such a structure have a resonance frequency at a wavelength that is larger than the structure itself? This is less surprising when we think about the cavity not as a set of boundary conditions for

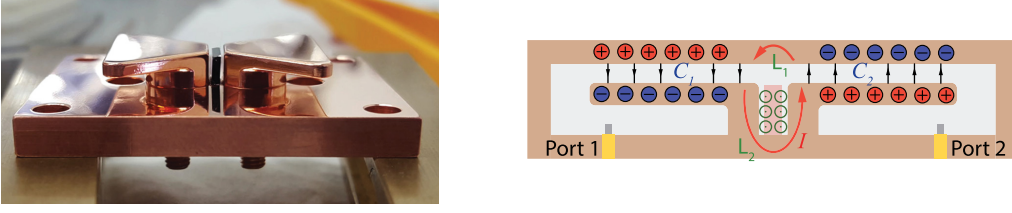


Figure 3.3.: 3D cavity. The two holes under the bow ties are mounts for standard SMA couplers.

photons but as an electrical circuit. In electronics the notion of a resonance circuit is common. Its idealized version consists of an inductance L and a capacitance C as depicted in fig. 3.2. Charge q flows back and forth between the two sides of the capacitance creating a magnetic field at the inductance. The Hamiltonian of this circuit consist of the sum of the energies in these two components

$$H = H_C + H_L = \frac{1}{2} \left(\frac{q^2}{C} + L\dot{q}^2 \right) = \frac{1}{2} \left(\tilde{q}^2 + CL\dot{\tilde{q}}^2 \right), \quad (3.2)$$

with $\tilde{q} = q/\sqrt{C}$. This is the Hamiltonian of a harmonic oscillator with a resonance frequency $\omega = 1/\sqrt{LC}$. It can be quantized in the usual way and thus serve as a bosonic mode. While the excitations are actually moving charge density fluctuations in the superconducting wire, they produce local electric and magnetic fields through which they can couple to the NV^- centers. These fields decay rapidly with the distance to the wire which leads to inhomogeneous coupling strengths.

The first experiments with NV^- centers and CPW cavities [28, 29, 59] were aiming at showing strong coupling between an excitation in the NV^- ensemble and the cavity mode [61]. They were performed in the low excitation regime where, as discussed in section 2.2.1, the Holstein-Primakoff approximation is valid and the ensemble of NV^- s can be approximated by a harmonic oscillator. In this regime only the effective coupling $g_{eff} = \sum_i^N g_i$, where g_i is the coupling of each individual NV^- center, enters the relevant dynamical equations. In this thesis however, we are interested in studying the dynamics for full inversion of the ensemble and the subsequent coherent oscillations between the ensemble and bosonic mode. The inhomogeneous coupling would lead to different time evolutions of each emitter wave function and thus break the coherence.

To obtain a homogeneous coupling to all NV^- centers a new cavity design had to be devised. The idea behind the CPW cavity was extended to the 3D case [62]. The new cavity is depicted in fig. 3.3. For obvious reasons it was called the "bow tie cavity". The magnetic field is focused in the volume between the two bow ties increasing the coupling to the NV^- ensemble.

Another important property of a resonator are its losses. In the case of an LC circuit they can be modeled with a resistance R , which corresponds to ohmic

resistance of the structure. Ideally the cavity should be made out of a material that becomes superconducting at the experimental conditions, like Aluminum. But a superconductor would block the external magnetic field that is needed to tune the energy levels of the NV^- center ground state in resonance with the cavity mode. Therefore, the cavity was made out of copper.

To be able to excite the ensemble of NV^- centers quickly we need to create a high field intensity within the cavity quickly. To understand how the various parameters influence the field intensity within the cavity we shortly discuss the *input-output formalism* [63]. We consider a two-port cavity that has internal losses κ_{int} and two ports that couple the cavity to external fields κ_1 and κ_2 . We can think of the cavity in terms of rate equations. The excitations that are in the cavity can leak out at a rate of $\kappa_{tot} = \kappa_{int} + \kappa_1 + \kappa_2$. But the excitations can also be replenished through an external drive. In the quantum mechanical treatment one usually classifies the cavity amplitude in terms of the number of excitations, i.e. a dimensionless number. It is useful to describe the drive in a similar way. However, since the drive consists of a traveling rather than a standing wave it is better to characterize it in terms of a photon flux rather than a photon number

$$P_{in} = \hbar\omega B_{in}^2. \quad (3.3)$$

This is the energy (averaged over $1/\omega$) that arrives at one of the cavity ports per unit time expressed as the energy per photon ($\hbar\omega$) times the photon flux B_{in}^2 . The rate equation for the complex cavity amplitude is

$$\dot{A} = (\kappa_{int} + \kappa_1 + \kappa_2)A + \sqrt{2\kappa_1}B_{in}. \quad (3.4)$$

We had to take the square root of the photon flux B_{in}^2 and as dimensional analysis dictates we also have to take the square root of the coupling because $[\kappa] = 1/[\text{time}]$. Note also that the drive "amplitude" couples with the coupling rate of the amplitude squared $2\kappa_1$ instead of just κ_1 [64, Eq. 4].¹ We obtain the steady state

$$A = \frac{\sqrt{2\kappa_1}}{\kappa_{int} + \kappa_1 + \kappa_2} B_{in}. \quad (3.6)$$

It is plotted in fig. 3.4. We see that the maximal cavity amplitude is reached when $\kappa_1 = \kappa_{int} + \kappa_2$. This maximum can be considerably higher than the drive

¹While it might seem easier to write down the rate equation for $a^\dagger a$, since it would not require one to take the square root of the photon flux, it actually is not. The interested reader is invited to solve the driven harmonic oscillator and arrive at

$$\frac{d}{dt} \langle a^\dagger a \rangle = -\gamma \langle a^\dagger a \rangle + if(t)(\langle a^\dagger(t) \rangle + \langle a(t) \rangle). \quad (3.5)$$

For the derivation we assumed that the driving term in the Hamiltonian looks like $H_D = \hbar f(t)(a^\dagger + a)$. One still needs the solution for the equations of motion for the complex amplitude $\langle a(t) \rangle$ to solve for $\langle a^\dagger a(t) \rangle$.

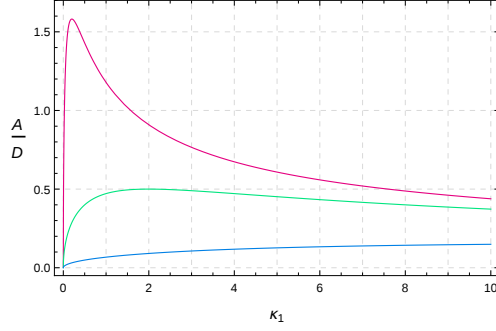


Figure 3.4.: The steady state cavity amplitude in units of the drive amplitude as a function of the drive coupling κ_1 for different values of $\kappa_{int} + \kappa_2 = 0.2, 2, 20$ (pink, green, blue).

amplitude. By using the following result from the input-output formalism [63, Eq. 5.2]

$$B_{out} = \sqrt{2\kappa_1}A - B_{in}, \quad (3.7)$$

where B_{out} denotes the amplitude of the reflected signal², we obtain

$$B_{out} = \frac{\kappa_{int} + \kappa_2 - \kappa_1}{\kappa_{int} + \kappa_2 + \kappa_1} B_{in}. \quad (3.8)$$

This allows us to classify three different regimes

Over-coupled: $\kappa_1 > \kappa_{int} + \kappa_2$, the reflected field is non-zero.

Critically-coupled: $\kappa_1 = \kappa_{int} + \kappa_2$, the reflected field from the cavity is zero and the cavity amplitude in the steady state reaches its maximum. In electronics terminology this is called "impedance matched".

Under-coupled: $\kappa_1 < \kappa_{int} + \kappa_2$, the reflected field is non-zero.

Note that the critical coupling is not always the optimal one. In the experiments that will be presented in the next chapter we apply short drive pulses and want the cavity to have the maximal number of excitations for a given pulse length and drive power. To obtain the optimal parameters for this case one needs to solve the full time dependent driven and damped harmonic oscillator problem and derive the optimal coupling as a function of the relevant parameters. An other interesting quantity is the transmitted amplitude. We define the input and output fields for the second port as in eq. (3.7)

$$C_{out} = \sqrt{2\kappa_2}A - C_{in}. \quad (3.9)$$

²Note that the relative sign of B_{in} and B_{out} is a matter of convention. It is different here as in [63] because we use a different convention in eq. (3.4) as compared to equation 2.13 in [63].

Since $C_{in} = 0$ we obtain for the transmission on resonance

$$C_{out} = \frac{2\sqrt{\kappa_2\kappa_1}}{\kappa_{int} + \kappa_2 + \kappa_1} B_{in}. \quad (3.10)$$

In electronics, an electrical circuit is usually classified through its inputs and outputs, also known as scattering parameters. They are defined as ratios of incoming and outgoing signals. In our notation this means

$$S_{11} = \frac{B_{out}}{B_{in}}, \quad S_{21} = \frac{C_{out}}{B_{in}}. \quad (3.11)$$

They are usually measured for a range of drive frequencies with a Vector Network Analyzer (VNA). They are complex linear quantities [65]. In our experiments we usually look at their absolute values on a logarithmic scale. The most convenient measurement is a measurement of the transmission, i.e. S_{21} , as a function of drive frequency. In this measurement one determines the resonance function of a driven harmonic oscillator, which is approximately a Lorentzian. This transmission function is related to the exponential decay of the cavity excitations through a Fourier transform. The relationship is described in appendix A. One can readily extract the total cavity decay rate from the width of this function. Resonators are classified according to their quality factor

$$Q = \frac{f_c}{\Delta f_{FWHM}} = \frac{\omega_c}{\Delta\omega_{FWHM}} = \frac{\pi f_c}{\kappa_{tot}} = \frac{\omega_c}{2\kappa_{tot}}. \quad (3.12)$$

The current cavity design consists of a total of five components: top, bottom, frame and the two parts of the bow tie. While performing the experiments for this thesis it was noted that the transmission on resonance is heavily dependent on how tightly the cavity screws are screwed in. This inspired the idea to build the cavity out of as few components as possible. Ideally the two bow ties would make up one piece with the cavity bottom.

4. Experimental Results

In this chapter we present some of the experimental data that was obtained during this thesis. We will show that the dynamics observed in the experiment are very well described by the semiclassical theory.

4.1. Measurement Scheme

Depending on the requirement of the experiment, the cavity is equipped with couplers of certain lengths. Then, the diamond is placed between the two bow ties and the cavity is assembled. Before the screws are fully tightened the cavity is connected to the Vector Network Analyzer (VNA) to determine its resonance frequency and transmission on resonance. If the resonance frequency is not within the desired range the cavity is disassembled and the bow ties are shifted. While monitoring the resonance function of the cavity on the VNA the screws are tightened, such that the transmission on resonance becomes maximal. Dirt, or improper alignment of the cavity parts can lead to low quality factors or low transmission on resonance. In this case the cavity needs to be reassembled again. The cavity quality factor decreases with increasing coupler length while the transmission on resonance increases. The quality factor of the cavity is also affected by the diamond. We have observed a decrease in the quality factor by more than 30% as compared to the bare cavity for certain diamonds. Typical resonance functions at this stage are shown in fig. 4.1.

Then the system is cooled down to 25mK in a dilution refrigerator. This process takes approximately 48 hours. The transmission function is measured again to determine the resonance frequency of the cavity. To tune one of the ground state transitions of the NV^- center in resonance with the cavity an external magnetic field is applied. The field is generated with superconducting Helmholtz coils. The transmission function is recorded for each field strength. When a transition of the NV^- center ground state becomes resonant with the cavity mode the resonance function either gets damped (weak coupling) or splits into two peaks (in the strong coupling regime). The field is adjusted such that the two peaks have the same height which is best visible in a linear plot. At this point the preparations for the experiment are complete.

The experiment consist of applying microwave pulses to one of the cavity ports and recording the time resolved output on the other port. Since the resonance frequency of the cavity is in the Gigahertz (GHz) range, this would require a time resolution on the scale of nanoseconds. However, the relevant information is not

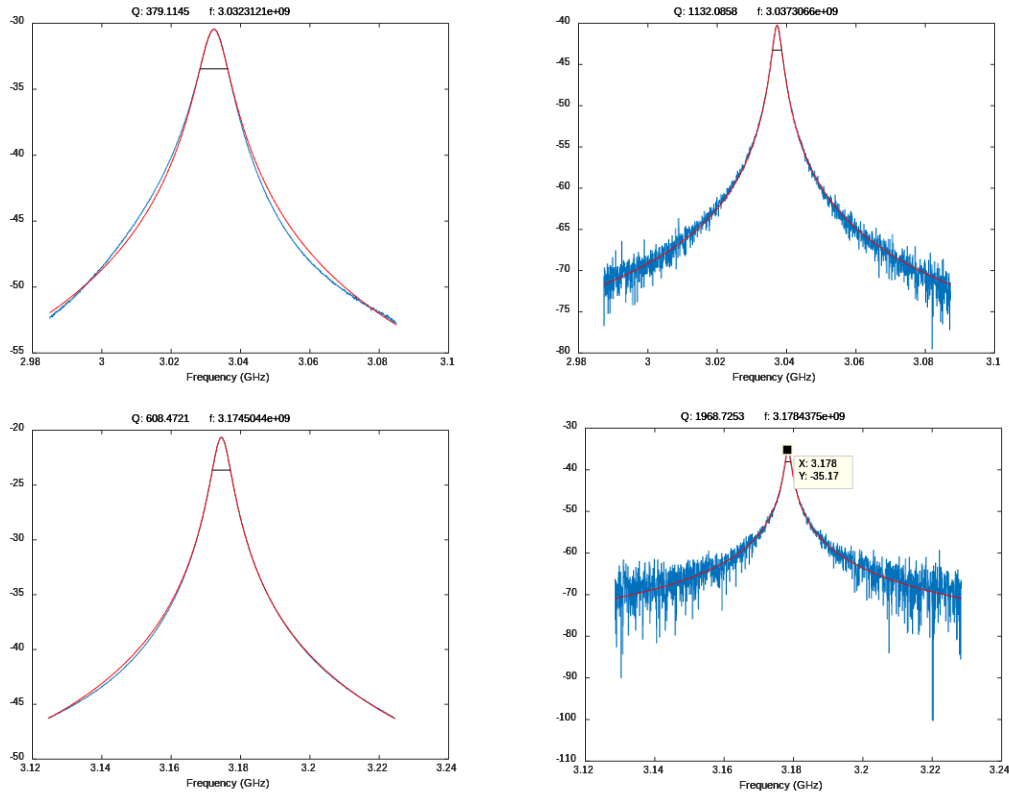


Figure 4.1.: Cavity resonance functions for symmetric couplers of length 1mm (upper panels) and 2mm (lower panels). Resonance functions at room temperature are shown on the left and at 25mK on the right. The resonance functions at low temperature include non negligible contributions from the cables that connect the cavity within the dilution refrigerator to the VNA. This leads to an apparent decrease of the transmission on resonance even though it has actually increased. Note also that the cables have different contributions for the upper and lower case and can not be accounted for with a single factor for both cases. One would expect the quality factor to be larger for short coupler lengths (upper panels). This is not the case here because different diamonds were used in the upper and lower cases which led to different damping.

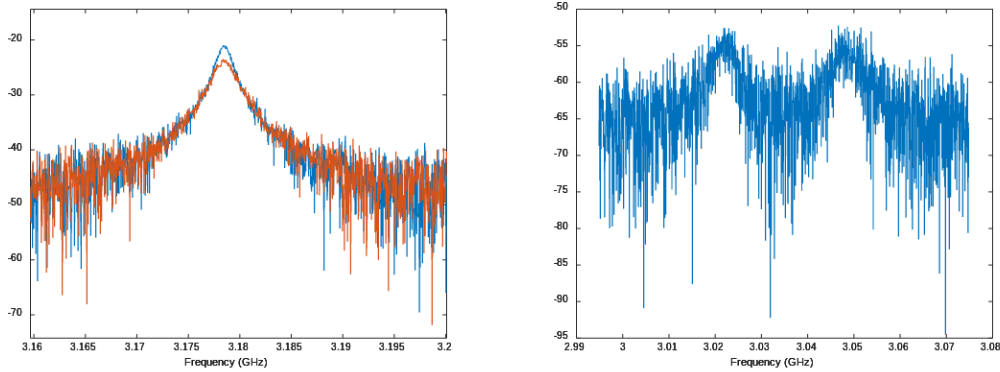


Figure 4.2.: Cavity resonance function in the weak (left) and strong (right) coupling regime. The blue curve in the left panel shows the transmission function for detuned NV^- centers for comparison.

contained in the GHz signal but rather in its envelope. Therefore, we employ a homodyne detection scheme which multiplies the output signal of the experiment with the input signal. The output of the experiment has the form

$$s(t) = I(t) \cos(\omega t) - Q(t) \sin(\omega t). \quad (4.1)$$

In the homodyne scheme this signal is split into two. One which is multiplied by the input signal $\cos(\omega t)$ and one that is multiplied with the input shifted by $\pi/2$, i.e. $\sin(\omega t)$. Frequencies that are higher than ω are filtered which results in two output signals $I(t)$ and $Q(t)$ respectively. The amplitude of the envelope is obtained by the formula

$$A(t) = \sqrt{I(t)^2 + Q(t)^2}. \quad (4.2)$$

This remedies the need for an oscilloscope in the GHz range in our experiment. This procedure is done by an IQ-mixer produced by Microcircuits. This transformation corresponds to the transformation into the rotating frame that we have done when deriving the Maxwell-Bloch equations in section 2.4.

4.2. Inversion of the NV^- ensemble

The experimental goal of this thesis is to go beyond the low-excitation limit where the Holstein-Primakoff approximation is valid and therefore to highly excite the NV^- ensemble. Our expectation was that the theoretical predictions from the Maxwell-Bloch equations should closely match our experimental observations, because the experimental system consists of a large number of weakly, but equally, coupled emitters. In the following we show that this is indeed the case.

In fig. 4.3 we present experimental data for a diamond with an NV^- density of approximately 40 ppm and therefore approximately 10^{17} defect centers in the

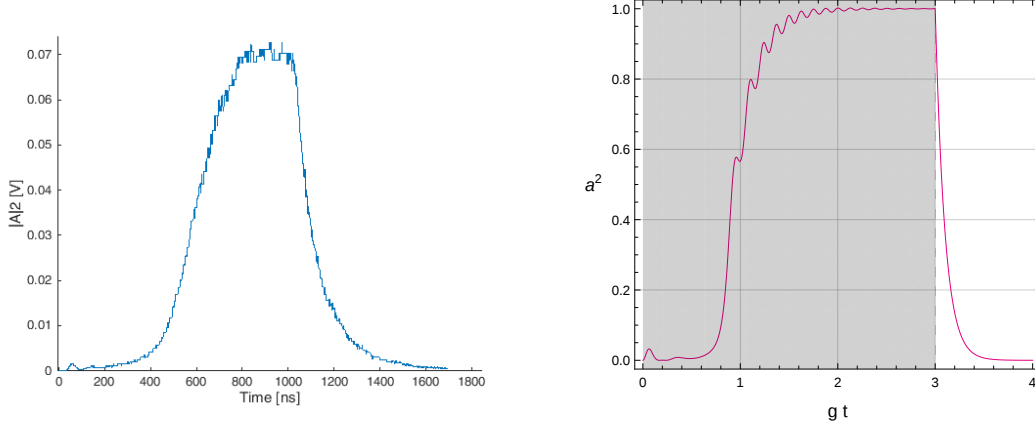


Figure 4.3.: The experimental (left) and theoretical (right) trace of the envelope of the cavity amplitude squared for an intermediate drive intensity. The shaded area in the right panel marks the time period when the drive is on.

cavity mode volume. Both cavity couplers had a length of 1mm and the cavity was resonantly driven for $1\mu\text{s}$. Initially one sees vacuum rabi oscillations around the low excitation state. Eventually the NV^- ensemble leaves the low excitation regime and a steep increase in the occupation number of the cavity is visible. This corresponds to the case shown in the upper panels of fig. 2.8. The theoretical prediction for the cavity amplitude is also reproduced in the right panel of fig. 4.3. The oscillations around the $\langle J_z \rangle = 0$, $\langle J_- \rangle = 0$ state are not visible in the experimental data because of the increased noise level at high cavity occupation. Based on the theoretical analysis it is clear that in this case the driving strength is not sufficient to invert the NV^- ensemble, i.e. achieve $\langle J_z \rangle > 0$.

Our setup already featured a 16 Watt microwave amplifier and a higher powered one was not available. To be able to achieve an inversion we could either replace the diamond sample with one that has a lower density of NV^- centers or change the couplers of the cavity. It is obvious that the output coupler should be chosen such that it provides sufficient coupling so that the signal arriving at the oscilloscope is large enough to be distinguished from the noise. At the same time the coupler should be small enough so that as few excitations are lost as possible. To fulfill these conditions a planar coupler was used at the output in the experiment that is presented in the following.

If the precise relation between the length of the coupler and coupling strength is known, then the input coupler length should be determined by solving the full driven harmonic oscillator model. It will depend on the desired pulse duration. But the coupler-length can also be determined empirically. For this experiment we used a 2mm coupler as the input. In fig. 4.4 the drive power is varied from -20dB of the maximal power to the maximal value for the case of two 1mm couplers (left panel) and asymmetric couplers as just described (right panel). A

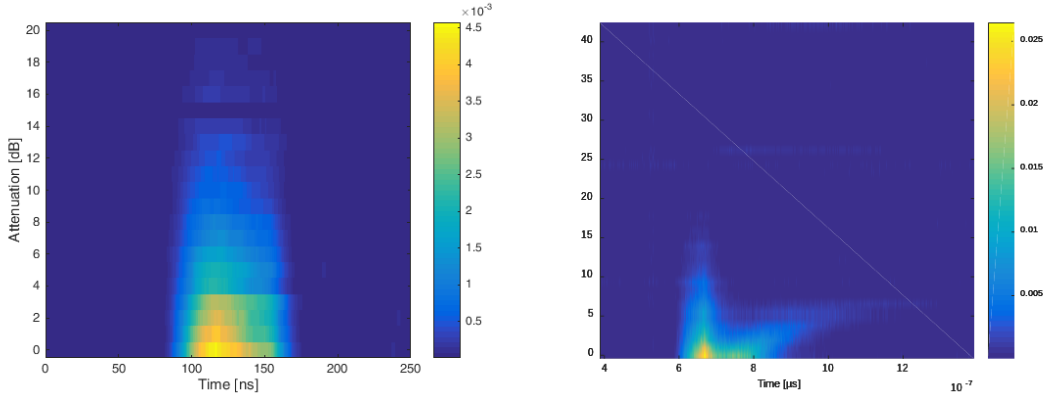


Figure 4.4.: The envelope of the cavity amplitude squared plotted over time for various drive powers. The left panel shows the data for the same setup as fig. 4.3, i.e. intermediate drive power. The right panel shows the data for an asymmetric coupler configuration.

branch-like structure emerges for the case of asymmetric couplers. Figure 4.5 shows an experiment where the duration of the drive-pulse is varied at fixed (in this case maximal) power - with the same setup as in the right panel of fig. 4.4. This time multiple branches are visible.

The explanation for this structure was partially presented in section 2.4.1. Figure 4.6 shows the numerical simulation of the Maxwell-Bloch equations for a single emitter and varying drive durations. The same branch structure as in the experiment is visible. The trace on the right shows the origin of the branch structure. For certain drive durations the system approaches its metastable state - an inverted dipole with zero excitations in the cavity mode. The closer the system comes to this state the longer the delay becomes leading to the branch structure. It is important to note that in the simulations only a single two-level system was considered. Therefore, the branch structure does not emerge because of coherence effects between multiple emitters. This explanation is different than the conclusion reached by the authors of [8]. Rose et. al. argue that the delay is caused by the same mechanism as discussed in section 2.5.3, i.e. consequent spontaneous emission with a changing dipole moment. This line of thinking is borrowed from the case of superradiance in vacuum. In this case however, the presence of photons in the cavity mode plays a crucial role since they prevent the system from reaching the metastable state and therefore lead to a decrease in the delay.

To be able to observe the branch structure the system has to reach the state $\langle a \rangle = 0$, $\langle J_z \rangle > 0$ and $\langle J_- \rangle = 0$. Crucially, the ensemble does not have to reach full inversion $\langle J_z \rangle = N$ as long as the polarization becomes 0 because of dephasing. Therefore, the presence of dephasing can decrease the minimal drive power that is needed to observe the branch structure.

For completeness we also show experimental data for another diamond sam-

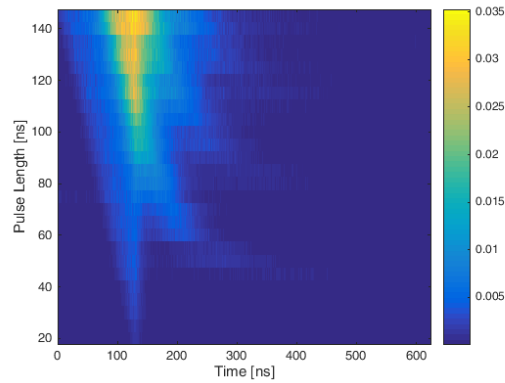


Figure 4.5.: The envelope of the cavity amplitude squared plotted over time for various drive pulse durations. In this case the drive power is sufficient to achieve $\langle J_z \rangle > 0$.

ple. This sample has approximately one order of magnitude less NV^- centers. Because of this an inversion can be reached at the same drive power as before and symmetric couplers. In this experiment the cavity the couplers had a length of 1mm. The data is shown in fig. 4.7.

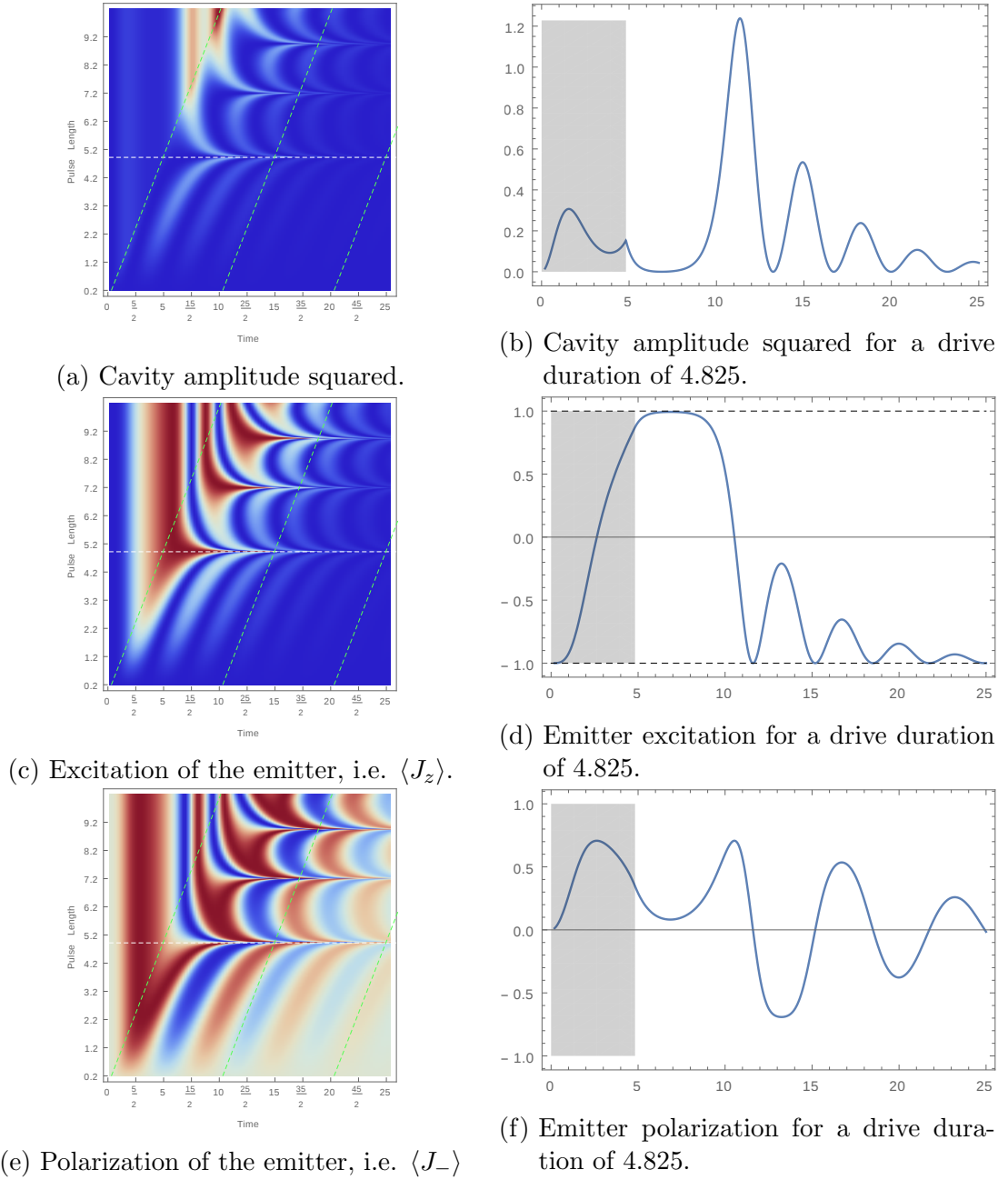


Figure 4.6.: Theoretical simulations of the cavity amplitude squared, the excitation and the polarization of a single emitter based on the Maxwell-Bloch equations. The panels on the right correspond to cuts through the plots on the left at the position marked by the white dashed line. The first green dashed line in the right panels signifies the moment in time when the drive is turned off. The shaded area in the right panels marks the duration of time when the drive is on. The units in the simulations are arbitrary as they serve to present the qualitative agreement of the semiclassical theory and the experiment.

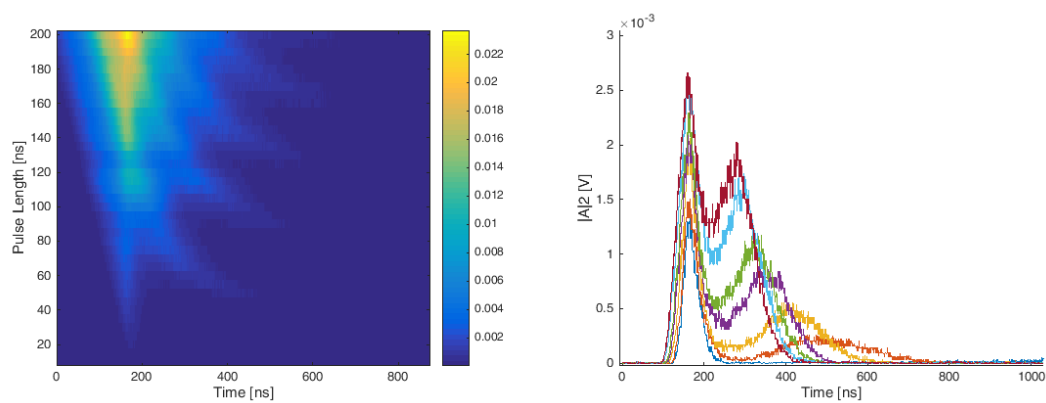


Figure 4.7.: The envelope of the cavity amplitude squared plotted over time for various pulse durations. In this experiment, rather than increasing the drive power another diamond was used that has fewer NV^- centers. The right panel shows individual traces from the lower branch in the right panel.

5. Conclusion

We have presented an overview of the models and methods that are relevant for the theoretical treatment of superradiance. A modern introduction to the phenomenon of superradiance was given, paying special attention to the difference of superradiance in vacuum and in a closed system. The close analogy to a classical dipole was explored to facilitate the intuitive understanding of the phenomenon. We discussed the three sources of nonlinearities that can appear in the treatment of the phenomenon.

First, we shortly discussed the quantum mechanical nonlinearity of the Tavis-Cummings model that appears due to the unequal coupling of the energy levels of the J_z operator to the bosonic mode. However, the dynamics of the coupled system is only affected by the energy difference of consequent transitions, i.e. by the anharmonicity of the energy transitions. As noted by Keeling [40] this anharmonicity becomes nearly undetectable for more than 10^6 emitters.

The second type of nonlinearity stems from the form of the Maxwell-Bloch equations and the fact that they have a metastable solution. This is equivalent to the nonlinearity of a pendulum and was discussed in section 2.4.1 as well as in section 2.5.4. The solution is given by a hyperbolic function. If more than one emitter is considered then the deviation from a harmonic oscillation becomes more pronounced. This can be considered as the third nonlinearity and was shortly discussed in section 2.5.5.

The theoretical work in this thesis was accompanied by an experiment with a novel type of 3D cavity that allowed the coherent excitation of a macroscopic ensemble of Nitrogen-Vacancy centers in a diamond. With this experimental setup we were able to successfully show the second type of nonlinearity. Beside a recent preprint by Rose et. al [8], this is the first time that this nonlinearity was shown experimentally.

This work provides a foundation for a range of further experiments. The experimental setup was equipped with a laser and a photo diode that can be used to determine the excitation of the NV^- ensemble and could provide a direct channel for the readout of the NV^- center state. Furthermore, the effects of spectral hole burning [29] can be explored in the coherent strong excitation regime.

Since our experimental setup was initially believed to be not powerful enough to achieve an inversion of the NV^- ensemble more efficient approaches to driving the ensemble were explored. In this context an exact solution for the driven Tavis-Cummings model was pursued. While these avenues seem very promising, further research is necessary to obtain conclusive results. The presentation of

these ideas was omitted because they exceed the scope of this thesis.

A. Relation of the Exponential Decay to the Cavity Linewidth

The Fourier transform of a Lorentzian is

$$\mathcal{F} \left(\frac{1}{\pi} \frac{\kappa/2\pi}{(f - f_0)^2 + (\kappa/2\pi)^2} \right) (t) = \exp [-2\pi i f_0 t - \kappa|t|]. \quad (\text{A.1})$$

Note that there are various definitions of the Fourier transform of which most differ only by a multiplicative factor. However, in eq. (A.1) the norm preserving Fourier transform with a factor of 2π in the exponent is used. This is convenient if one transforms to the frequency domain because the factor from the fourier transform contains a $2\pi f t$ and the factor from the description of the oscillation in the time domain contains $2\pi f_0 t$ which gives the term $(f - f_0)^2$ in the Lorentzian. If we were transforming to the angular frequency domain the fourier factor would have $2\pi\omega t$ while the oscillatory term would have either $\omega_0 t$ or $2\pi\omega_0 t$. In the former case we would get a term like $(\omega - \omega_0/2\pi)^2$ and in the latter case the ω_0 wouldnt actually correspond to the angular frequency of the wave. If we transform to the angular frequency domain by using a fourier transform with a factor of ωt in the exponent we would get the following

$$\mathcal{F} \left(\frac{1}{\pi} \frac{\kappa}{(\omega - \omega_0)^2 + \kappa^2} \right) (t) = \exp [i\omega_0 t - \kappa|t|]. \quad (\text{A.2})$$

Thus, the decay rate is related to the FWHM Δf by $\kappa = \pi\Delta f_{FWHM}$ or by $\kappa = \Delta\omega_{HWHM}$. For the Quality factor we have the following relations

$$Q = \frac{f_c}{\Delta f_{FWHM}} = \frac{\omega_c}{\Delta\omega_{FWHM}} = \frac{\pi f_c}{\kappa} = \frac{\omega_c}{2\kappa}. \quad (\text{A.3})$$

This κ denotes the decay rate of the amplitude and thus corresponds to the κ in the Maxwell-Bloch equation for the cavity amplitude eq. (2.62).

Bibliography

- [1] R. H. Dicke. „Coherence in Spontaneous Radiation Processes“. In: *Physical Review* 93.1 (Jan. 1954), pp. 99–110. ISSN: 0031-899X. DOI: [10.1103/PhysRev.93.99](https://doi.org/10.1103/PhysRev.93.99).
- [2] D. Meiser et al. „Prospects for a millihertz-linewidth laser“. In: *Physical Review Letters* 102.16 (2009), pp. 1–4. ISSN: 00319007. DOI: [10.1103/PhysRevLett.102.163601](https://doi.org/10.1103/PhysRevLett.102.163601). arXiv: [arXiv:0901.3105v2](https://arxiv.org/abs/0901.3105v2).
- [3] Peter Domokos and Helmut Ritsch. „Collective Cooling and Self-Organization of Atoms in a Cavity“. In: *Physical Review Letters* 89.25 (Dec. 2002), p. 253003. ISSN: 0031-9007. DOI: [10.1103/PhysRevLett.89.253003](https://doi.org/10.1103/PhysRevLett.89.253003).
- [4] D. Nagy, G. Szirmai, and P. Domokos. „Self-organization of a Bose-Einstein condensate in an optical cavity“. In: *The European Physical Journal D* 48.1 (June 2008), pp. 127–137. ISSN: 1434-6060. DOI: [10.1140/epjd/e2008-00074-6](https://doi.org/10.1140/epjd/e2008-00074-6).
- [5] Kristian Baumann et al. „Dicke quantum phase transition with a superfluid gas in an optical cavity“. In: *Nature* 464.7293 (Apr. 2010), pp. 1301–1306. ISSN: 0028-0836. DOI: [10.1038/nature09009](https://doi.org/10.1038/nature09009).
- [6] L. J. Zou et al. „Implementation of the Dicke Lattice Model in Hybrid Quantum System Arrays“. In: *Physical Review Letters* 113.2 (July 2014), p. 023603. ISSN: 0031-9007. DOI: [10.1103/PhysRevLett.113.023603](https://doi.org/10.1103/PhysRevLett.113.023603).
- [7] Rodolfo Bonifacio and Giuliano Preparata. „Coherent Spontaneous Emission“. In: *Physical Review A* 2.2 (Aug. 1970), pp. 336–347. ISSN: 0556-2791. DOI: [10.1103/PhysRevA.2.336](https://doi.org/10.1103/PhysRevA.2.336).
- [8] B C Rose et al. „Coherent Rabi dynamics of a superradiant spin ensemble in a microwave cavity“. In: (Feb. 2017), pp. 1–9. arXiv: [1702.00504](https://arxiv.org/abs/1702.00504).
- [9] Liang Jin et al. „Proposal for a room-temperature diamond maser“. In: *Nature Communications* 6 (Sept. 2015), p. 8251. ISSN: 2041-1723. DOI: [10.1038/ncomms9251](https://doi.org/10.1038/ncomms9251).
- [10] A. D. Ludlow et al. „Sr Lattice Clock at 1×10^{-16} Fractional Uncertainty by Remote Optical Evaluation with a Ca Clock“. In: *Science* 319.5871 (Mar. 2008), pp. 1805–1808. ISSN: 0036-8075. DOI: [10.1126/science.1153341](https://doi.org/10.1126/science.1153341).
- [11] Ichiro Ushijima et al. „Cryogenic optical lattice clocks“. In: *Nature Photonics* 9.3 (Feb. 2015), pp. 185–189. ISSN: 1749-4885. DOI: [10.1038/nphoton.2015.5](https://doi.org/10.1038/nphoton.2015.5).

- [12] B. J. Bloom et al. „An optical lattice clock with accuracy and stability at the 10^{-18} level“. In: *Nature* 506.7486 (Jan. 2014), pp. 71–75. ISSN: 0028-0836. DOI: [10.1038/nature12941](https://doi.org/10.1038/nature12941).
- [13] S Kolkowitz et al. „Gravitational wave detection with optical lattice atomic clocks“. In: *Physical Review D* 94.12 (Dec. 2016), p. 124043. ISSN: 2470-0010. DOI: [10.1103/PhysRevD.94.124043](https://doi.org/10.1103/PhysRevD.94.124043).
- [14] J. D. Teufel et al. „Sideband cooling of micromechanical motion to the quantum ground state“. In: *Nature* 475.7356 (July 2011), pp. 359–363. ISSN: 0028-0836. DOI: [10.1038/nature10261](https://doi.org/10.1038/nature10261).
- [15] Kenji Numata, Amy Kemery, and Jordan Camp. „Thermal-Noise Limit in the Frequency Stabilization of Lasers with Rigid Cavities“. In: *Physical Review Letters* 93.25 (Dec. 2004), p. 250602. ISSN: 0031-9007. DOI: [10.1103/PhysRevLett.93.250602](https://doi.org/10.1103/PhysRevLett.93.250602).
- [16] Mark Notcutt et al. „Contribution of thermal noise to frequency stability of rigid optical cavity via Hertz-linewidth lasers“. In: *Physical Review A* 73.3 (Mar. 2006), p. 031804. ISSN: 1050-2947. DOI: [10.1103/PhysRevA.73.031804](https://doi.org/10.1103/PhysRevA.73.031804).
- [17] Christian Hagemann et al. „Ultrastable laser with average fractional frequency drift rate below $5 \cdot 10^{-19}/s$ “. In: *Optics Letters* 39.17 (Sept. 2014), p. 5102. ISSN: 0146-9592. DOI: [10.1364/OL.39.005102](https://doi.org/10.1364/OL.39.005102).
- [18] Justin G Bohnet et al. „A steady-state superradiant laser with less than one intracavity photon“. In: *Nature* 484.7392 (Apr. 2012), pp. 78–81. ISSN: 0028-0836. DOI: [10.1038/nature10920](https://doi.org/10.1038/nature10920).
- [19] Matthew A Norcia et al. „Superradiance on the millihertz linewidth strontium clock transition“. In: *Science Advances* 2.10 (Oct. 2016), e1601231–e1601231. ISSN: 2375-2548. DOI: [10.1126/sciadv.1601231](https://doi.org/10.1126/sciadv.1601231). arXiv: [arXiv: 1603.05671v1](https://arxiv.org/abs/1603.05671v1).
- [20] Mark Oxborrow, Jonathan D Breeze, and Neil M Alford. „Room-temperature solid-state maser“. In: *Nature* 488.7411 (2012), pp. 353–356. ISSN: 0028-0836. DOI: [10.1038/nature11339](https://doi.org/10.1038/nature11339).
- [21] E. Schrödinger. „ARE THERE QUANTUM JUMPS ?“ In: *The British Journal for the Philosophy of Science* III.11 (1952), pp. 233–242. ISSN: 0007-0882. DOI: [10.1093/bjps/III.11.233](https://doi.org/10.1093/bjps/III.11.233).
- [22] Herbert Walther et al. „Cavity quantum electrodynamics“. In: *Reports on Progress in Physics* 69.5 (May 2006), pp. 1325–1382. ISSN: 0034-4885. DOI: [10.1088/0034-4885/69/5/R02](https://doi.org/10.1088/0034-4885/69/5/R02).
- [23] D. Deutsch. „Quantum Theory, the Church-Turing Principle and the Universal Quantum Computer“. In: *Proceedings of the Royal Society A: Mathematical, Physical and Engineering Sciences* 400.1818 (July 1985), pp. 97–117. ISSN: 1364-5021. DOI: [10.1098/rspa.1985.0070](https://doi.org/10.1098/rspa.1985.0070).

- [24] I. Diniz et al. „Strongly coupling a cavity to inhomogeneous ensembles of emitters: Potential for long-lived solid-state quantum memories“. In: *Physical Review A - Atomic, Molecular, and Optical Physics* 84.6 (2011), pp. 1–9. ISSN: 10502947. DOI: [10.1103/PhysRevA.84.063810](https://doi.org/10.1103/PhysRevA.84.063810). arXiv: [1101.1842](https://arxiv.org/abs/1101.1842).
- [25] Brian Julsgaard and Klaus Mølmer. „Dynamical evolution of an inverted spin ensemble in a cavity: Inhomogeneous broadening as a stabilizing mechanism“. In: *Physical Review A* 86.6 (Dec. 2012), p. 063810. ISSN: 1050-2947. DOI: [10.1103/PhysRevA.86.063810](https://doi.org/10.1103/PhysRevA.86.063810).
- [26] P. Rabl et al. „Hybrid quantum processors: Molecular ensembles as quantum memory for solid state circuits“. In: *Physical Review Letters* 97.3 (2006), pp. 1–4. ISSN: 00319007. DOI: [10.1103/PhysRevLett.97.033003](https://doi.org/10.1103/PhysRevLett.97.033003). arXiv: [0604140](https://arxiv.org/abs/0604140) [quant-ph].
- [27] C. Grezes et al. „Multimode Storage and Retrieval of Microwave Fields in a Spin Ensemble“. In: *Physical Review X* 4.2 (2014), p. 021049. ISSN: 2160-3308. DOI: [10.1103/PhysRevX.4.021049](https://doi.org/10.1103/PhysRevX.4.021049).
- [28] S. Putz et al. „Protecting a spin ensemble against decoherence in the strong-coupling regime of cavity QED“. In: *Nature Physics* (Aug. 2014). ISSN: 1745-2473. DOI: [10.1038/nphys3050](https://doi.org/10.1038/nphys3050).
- [29] Stefan Putz et al. „Spectral hole burning and its application in microwave photonics“. In: *Nature Photonics* 11.1 (Nov. 2016), pp. 36–39. ISSN: 1749-4885. DOI: [10.1038/nphoton.2016.225](https://doi.org/10.1038/nphoton.2016.225). arXiv: [1512.00248](https://arxiv.org/abs/1512.00248).
- [30] Matthew Reagor et al. „Quantum memory with millisecond coherence in circuit QED“. In: *Physical Review B* 94.1 (July 2016), p. 014506. ISSN: 2469-9950. DOI: [10.1103/PhysRevB.94.014506](https://doi.org/10.1103/PhysRevB.94.014506). arXiv: [1508.05882](https://arxiv.org/abs/1508.05882).
- [31] P. C. Maurer et al. „Room-Temperature Quantum Bit Memory Exceeding One Second“. In: *Science* 336.6086 (June 2012), pp. 1283–1286. ISSN: 0036-8075. DOI: [10.1126/science.1220513](https://doi.org/10.1126/science.1220513).
- [32] H. J. Carmichael. *Statistical Methods in Quantum Optics 1. Master Equations and Fokker-Planck Equations*. 1. ed. Texts and monographs in physics. Berlin [u.a.]: Springer, 2002. ISBN: 3-540-54882-3.
- [33] E. T. Jaynes and F W Cummings. „Comparison of quantum and semiclassical radiation theories with application to the beam maser“. In: *Proceedings of the IEEE* 51.1 (1963), pp. 89–109. ISSN: 0018-9219. DOI: [10.1109/PROC.1963.1664](https://doi.org/10.1109/PROC.1963.1664).
- [34] T Niemczyk et al. „Circuit quantum electrodynamics in the ultrastrong-coupling regime“. In: *Nature Physics* 6.10 (Oct. 2010), pp. 772–776. ISSN: 1745-2473. DOI: [10.1038/nphys1730](https://doi.org/10.1038/nphys1730).

- [35] Michael Tavis and Frederick W Cummings. „Exact Solution for an N Molecule Radiation-Field Hamiltonian“. In: *Physical Review* 170.2 (June 1968), pp. 379–384. ISSN: 0031-899X. DOI: [10.1103/PhysRev.170.379](https://doi.org/10.1103/PhysRev.170.379).
- [36] R. Thompson et al. „Nonlinear spectroscopy in the strong-coupling regime of cavity QED“. In: *Physical Review A* 57.4 (1998), pp. 3084–3104. ISSN: 1050-2947. DOI: [10.1103/PhysRevA.57.3084](https://doi.org/10.1103/PhysRevA.57.3084).
- [37] Barry M Garraway. „The Dicke model in quantum optics: Dicke model revisited“. In: *Philosophical Transactions of the Royal Society A: Mathematical, Physical and Engineering Sciences* 369.1939 (Mar. 2011), pp. 1137–1155. ISSN: 1364-503X. DOI: [10.1098/rsta.2010.0333](https://doi.org/10.1098/rsta.2010.0333).
- [38] T. Holstein and H. Primakoff. „Field dependence of the intrinsic domain magnetization of a ferromagnet“. In: *Physical Review* 58.12 (1940), pp. 1098–1113. ISSN: 0031899X. DOI: [10.1103/PhysRev.58.1098](https://doi.org/10.1103/PhysRev.58.1098). arXiv: [arXiv: 1011.1669v3](https://arxiv.org/abs/1011.1669v3).
- [39] Dmitry O. Krimer et al. „Non-Markovian dynamics of a single-mode cavity strongly coupled to an inhomogeneously broadened spin ensemble“. In: *Physical Review A* 90.4 (Oct. 2014), p. 043852. ISSN: 1050-2947. DOI: [10.1103/PhysRevA.90.043852](https://doi.org/10.1103/PhysRevA.90.043852). arXiv: [1410.0728](https://arxiv.org/abs/1410.0728).
- [40] Jonathan Keeling. „Quantum corrections to the semiclassical collective dynamics in the Tavis-Cummings model“. In: *Physical Review A* 79.5 (May 2009), p. 053825. ISSN: 1050-2947. DOI: [10.1103/PhysRevA.79.053825](https://doi.org/10.1103/PhysRevA.79.053825). arXiv: [arXiv:0901.4245v2](https://arxiv.org/abs/0901.4245v2).
- [41] H. J. Carmichael. *Statistical Methods in Quantum Optics 2. Non-classical Fields*. 1. ed. Theoretical and mathematical physics; Texts and monographs in physics. Berlin [u.a.]: Springer, 2008. ISBN: 978-3-642-09041-7.
- [42] Dmitry O. Krimer, Benedikt Hartl, and Stefan Rotter. „Hybrid Quantum Systems with Collectively Coupled Spin States: Suppression of Decoherence through Spectral Hole Burning“. In: *Physical Review Letters* 115.3 (July 2015), p. 033601. ISSN: 0031-9007. DOI: [10.1103/PhysRevLett.115.033601](https://doi.org/10.1103/PhysRevLett.115.033601). arXiv: [1501.03487](https://arxiv.org/abs/1501.03487).
- [43] M. Gross and S. Haroche. „Superradiance: An essay on the theory of collective spontaneous emission“. In: *Physics Reports* 93.5 (Dec. 1982), pp. 301–396. ISSN: 03701573. DOI: [10.1016/0370-1573\(82\)90102-8](https://doi.org/10.1016/0370-1573(82)90102-8).
- [44] Ching Tsung Lee. „Exact solution of the superradiance master equation. I. Complete initial excitation“. In: *Physical Review A* 15.5 (May 1977), pp. 2019–2031. ISSN: 0556-2791. DOI: [10.1103/PhysRevA.15.2019](https://doi.org/10.1103/PhysRevA.15.2019).
- [45] Ching Tsung Lee. „Exact solution of the superradiance master equation. II. Arbitrary initial excitation“. In: *Physical Review A* 16.1 (July 1977), pp. 301–312. ISSN: 0556-2791. DOI: [10.1103/PhysRevA.16.301](https://doi.org/10.1103/PhysRevA.16.301).

- [46] Wikipedia. *Pendulum (mathematics)* - *Wikipedia The Free Encyclopedia*. 2017. URL: [https://en.wikipedia.org/wiki/Pendulum%7B%5C_%7D\(mathematics\)](https://en.wikipedia.org/wiki/Pendulum%7B%5C_%7D(mathematics)) (visited on 02/22/2017).
- [47] S. L. McCall and E. L. Hahn. „Self-Induced Transparency by Pulsed Coherent Light“. In: *Physical Review Letters* 18.21 (May 1967), pp. 908–911. ISSN: 0031-9007. DOI: [10.1103/PhysRevLett.18.908](https://doi.org/10.1103/PhysRevLett.18.908).
- [48] Yu. A. Il’Inskii and N. S. Maslova. „The classical analog of superradiation in a system of interacting nonlinear oscillators“. In: *Zhurnal Eksperimentalnoi i Teoreticheskoi Fiziki* 94 (1988), pp. 171–174.
- [49] Neill Lambert et al. „Superradiance with an ensemble of superconducting flux qubits“. In: (Nov. 2016), pp. 1–8. DOI: [10.1103/PhysRevB.94.224510](https://doi.org/10.1103/PhysRevB.94.224510). arXiv: [1611.07104](https://arxiv.org/abs/1611.07104).
- [50] J A Mlynek et al. „Observation of Dicke superradiance for two artificial atoms in a cavity with high decay rate“. In: *Nature Communications* 5 (2014), pp. 1–6. ISSN: 2041-1723. DOI: [10.1038/ncomms6186](https://doi.org/10.1038/ncomms6186). arXiv: [1412.2392](https://arxiv.org/abs/1412.2392).
- [51] Kae Nemoto et al. „Photonic Quantum Networks formed from NV centers“. In: *Scientific Reports* 6.May (2016), p. 26284. ISSN: 2045-2322. DOI: [10.1038/srep26284](https://doi.org/10.1038/srep26284). arXiv: [1412.5950](https://arxiv.org/abs/1412.5950).
- [52] B Hensen et al. „Loophole-free Bell inequality violation using electron spins separated by 1.3 kilometres“. In: *Nature* 526.7575 (Oct. 2015), pp. 682–686. ISSN: 0028-0836.
- [53] B Hensen et al. „Loophole-free Bell test using electron spins in diamond: second experiment and additional analysis“. In: *Scientific Reports* 6 (Aug. 2016), p. 30289.
- [54] Lachlan J. Rogers et al. „All-Optical Initialization, Readout, and Coherent Preparation of Single Silicon-Vacancy Spins in Diamond“. In: *Physical Review Letters* 113.26 (Dec. 2014), p. 263602. ISSN: 0031-9007. DOI: [10.1103/PhysRevLett.113.263602](https://doi.org/10.1103/PhysRevLett.113.263602).
- [55] G Davies and INSPEC (Information Service). *Properties and Growth of Diamond*. EMIS datareviews series. INSPEC, the Institution of Electrical Engineers, 1994. ISBN: 9780852968758.
- [56] Tobias Nöbauer et al. „Creation of ensembles of nitrogen-vacancy centers in diamond by neutron and electron irradiation“. In: (Sept. 2013), pp. 1–12. arXiv: [1309.0453](https://arxiv.org/abs/1309.0453).
- [57] Adam Gali, Maria Fyta, and Efthimios Kaxiras. „Ab initio supercell calculations on nitrogen-vacancy center in diamond: Electronic structure and hyperfine tensors“. In: *Physical Review B* 77.15 (Apr. 2008), p. 155206. ISSN: 1098-0121. DOI: [10.1103/PhysRevB.77.155206](https://doi.org/10.1103/PhysRevB.77.155206).

- [58] E van Oort, N B Manson, and M Glasbeek. „Optically detected spin coherence of the diamond N-V centre in its triplet ground state“. In: *Journal of Physics C: Solid State Physics* 21.23 (Aug. 1988), pp. 4385–4391. ISSN: 0022-3719. DOI: [10.1088/0022-3719/21/23/020](https://doi.org/10.1088/0022-3719/21/23/020).
- [59] R. Amsüss et al. „Cavity QED with Magnetically Coupled Collective Spin States“. In: *Physical Review Letters* 107.6 (Aug. 2011), p. 060502. ISSN: 0031-9007. DOI: [10.1103/PhysRevLett.107.060502](https://doi.org/10.1103/PhysRevLett.107.060502). arXiv: [1103.1045](https://arxiv.org/abs/1103.1045).
- [60] J Majer et al. „Coupling superconducting qubits via a cavity bus.“ In: *Nature* 449.7161 (2007), pp. 443–447. ISSN: 0028-0836. DOI: [10.1038/nature06184](https://doi.org/10.1038/nature06184). arXiv: [0709.2135](https://arxiv.org/abs/0709.2135).
- [61] K. Sandner et al. „Strong magnetic coupling of an inhomogeneous nitrogen-vacancy ensemble to a cavity“. In: *Physical Review A* 85.5 (May 2012), p. 053806. ISSN: 1050-2947. DOI: [10.1103/PhysRevA.85.053806](https://doi.org/10.1103/PhysRevA.85.053806). arXiv: [1112.4767](https://arxiv.org/abs/1112.4767).
- [62] Andreas Angerer et al. „Collective strong coupling with homogeneous Rabi frequencies using a 3D lumped element microwave resonator“. In: *Applied Physics Letters* 109.3 (2016). ISSN: 00036951. DOI: [10.1063/1.4959095](https://doi.org/10.1063/1.4959095). arXiv: [1605.05554](https://arxiv.org/abs/1605.05554).
- [63] C. W. Gardiner and M. J. Collett. „Input and output in damped quantum systems: Quantum stochastic differential equations and the master equation“. In: *Physical Review A* 31.6 (June 1985), pp. 3761–3774. ISSN: 0556-2791. DOI: [10.1103/PhysRevA.31.3761](https://doi.org/10.1103/PhysRevA.31.3761).
- [64] Markus Aspelmeyer, Tobias J. Kippenberg, and Florian Marquardt. „Cavity optomechanics“. In: *Reviews of Modern Physics* 86.4 (2014), pp. 1391–1452. ISSN: 15390756. DOI: [10.1103/RevModPhys.86.1391](https://doi.org/10.1103/RevModPhys.86.1391). arXiv: [0712.1618](https://arxiv.org/abs/0712.1618).
- [65] Agilent Technologies. *Agilent Network Analyzer Basics*. URL: <http://cp.literature.agilent.com/litweb/pdf/5965-%7B%7D0A7917E.pdf>.